IN VITRO EFFECTS OF CHLORPYRIFOS OXON ON PEROXISOME PROLIFERATOR-ACTIVATED SIGNALING IN MCF-7 CELLS

By

STACEY HERRIAGE

Bachelor of Arts in General Studies

Northeastern State University

Tahlequah, Oklahoma

2013

Submitted to the Faculty of the
Graduate College of the
Oklahoma State University
in partial fulfillment of
the requirements for
the Degree of
MASTER OF SCIENCE
December, 2019

IN VITRO EFFECTS OF CHLORPYRIFOS OXON ON PEROXISOME PROLIFERATOR-ACTIVATED SIGNALING IN MCF-7 CELLS

Thesis Approved:

Dr. Carey Pope

Thesis Adviser

Dr. Guangping Chen

Dr. Lara Maxwell

ACKNOWLEDGEMENTS

I would like to express my very great appreciation to Dr. Carey Pope for his expert guidance as my advisor, his good humor, and seemingly infinite patience. Additionally, I would like to thank committee members Dr. Guangping Chen and Dr. Lara Maxwell for their time and instruction. I am so fortunate to have the opportunity to learn from such an amazing and knowledgeable group mentors.

Last, but not least, I would like to express my tremendous gratitude to my family, my friends, and to Bee Bee my beagle dog, for their unwavering support and encouragement.

Name: STACEY HERRIAGE

Date of Degree: DECEMBER, 2019

Title of Study: IN VITRO EFFECTS OF CHLORPYRIFOS OXON ON PEROXISOME PROLIFERATOR-ACTIVATED SIGNALING IN MCF-7 CELLS

Major Field: VETERINARY BIOMEDICAL SCIENCES

Abstract: The U.S. population is chronically exposed to a wide variety of environmental chemicals, including organophosphorus pesticides (OPs) such as chlorpyrifos. Chlorpyrifos oxon (CPO), the active metabolite of chlorpyrifos, inhibits acetylcholinesterase (AChE) to elicit toxicity, but is also a potent inhibitor of fatty acid amide hydrolase (FAAH). FAAH plays an important role in the degradation of fatty acid signaling lipids, and is the key enzyme in terminating endocannabinoid (eCB) signaling by hydrolyzing N-archidonylethanolamine (anandamide, AEA). AEA and other lipid intermediates, such as the eCB-like metabolites oleoylethanolamide (OEA) and palmitoylethanolamide (PEA), are potent agonists at peroxisome proliferator-activated receptors (PPAR). PPARs regulate genes involved in numerous physiological processes associated with lipid metabolism and energy homeostasis. We hypothesized that inhibition of FAAH by CPO would disrupt degradation of intracellular AEA and OEA, leading to increased PPAR transcriptional activity, and altered expression of PPAR target genes. To evaluate the effects of CPO on PPAR-mediated gene expression, we exposed MCF-7 cells to a range of CPO concentrations in culture. In vitro inhibition assays were first conducted to evaluate concentration-dependent inhibition of FAAH and, for comparison, AChE. Cell cultures were then exposed to one of three selected CPO concentrations either alone, or along with AEA or OEA. Samples were collected at 8 hours, 1 day, and 3 days after dosing for gene expression analysis. Changes in expression of four selected target genes coupled to PPAR activation were measured using real-time quantitative polymerase chain reaction, and the comparative Ct method to quantify fold change in expression. Our results demonstrated inhibition of FAAH and AChE, as well as upregulation of all four target genes in a concentration and time-dependent manner. Inclusion of either AEA or OEA with CPO generally decreased the extent of gene upregulation noted with CPO alone. These are the first data to suggest that exposure to chlorpyrifos could influence lipid metabolism through PPAR activation, potentially contributing to metabolic disorders including obesity.

TABLE OF CONTENTS

LIST OF TABLES

Table Page

LIST OF FIGURES

Figure Page

Figure Page

CHAPTER I

INTRODUCTION

Chronic exposure to biologically active environmental contaminants is something that is unavoidable. Despite some of their known toxicological effects, many such contaminants exist in our home, in the workplace, and in our food and water sources, just to name a few. For example, organophosphorus compounds are used in many forms that, are not only useful, such as in plasticizers, but also those designed to keep us safe, such as flame retardants and pesticides created to protect our food crops (1).

An organophosphorus compound (OP) is defined as any member of a group of organic compounds containing a phosphorus atom. Originally, OP synthesis was carried out with the goal of creating new, effective pesticides for the protection of food crops from insect infestation (1,2). Tetraetylpyrophosphate (TEPP) was the first commercially available OP insecticide, first synthesized circa 1854 (3). The first OP chemical weapon was synthesized in December of 1936. While working to create a new formulation of an OP insecticide, due to the shortage of the common insecticide of the time, nicotine, German scientist Gerhard Schrader accidentally made tabun (Ethyl dimethylphosphoramidocyanidate), which became the first of the so-called G-agents (G for Germany) (3).

Two additional G-agents (sarin and soman) were synthesized by the same group shortly after, which were followed by a second generation of nerve agents, known as the V-agents (V for venom) (4). The focus on creating more effective weapons for some years gave way to a decline in OP pesticide synthesis. However, after the publication of "Silent Spring" by Rachel Carson in 1962, which ultimately led to the ban of the popular and widely used organochlorine insecticide DDT, it became necessary to find new chemicals to control insect pests. Once again, OPs became the most popular candidates for research and development in this capacity. In 1965, Dow AgroSciences got market the now common insecticide chlorpyrifos.

Chlorpyrifos (CPF; O,O'-diethyl-3,5,6-trichloropyridinyl-phosphorothioate) is one of the most extensively used insecticides worldwide, although it has been banned for residential use in the United States (5). It remains extensively used in industrial agriculture. Additionally, it is used for protection of non-structural wood products, to combat insects that pose a threat to public health, such as municipal mosquito control spraying, and is actually the most frequently applied insecticide on golf courses. Its broad spectrum efficacy as an insecticide, combined with cost-effective availability, and user-friendly ease of application, has made chlorpyrifos a popular pesticide for a variety of purposes. Although risks to non-target organisms, including humans, have been extensively studied for safety and regulatory reasons, potential adverse effects of environmental exposure to chlorpyrifos remains a topic of concern for public health (4,6,7).

For humans, routes of exposure to chlorpyrifos include dermal, inhalation, and ingestion, with ingestion being the major route of entry (8). Only after chlorpyrifos has

been absorbed it is metabolically converted to its highly reactive metabolite, chlorpyrifos oxon, through oxidative desulfuration (9). Figure 1 illustrates this reaction. If one consumes produce containing chlorpyrifos residues, the parent insecticide is converted to the oxon in the liver or other organ, which is roughly 1,000 times more potent than the insecticide itself (9).

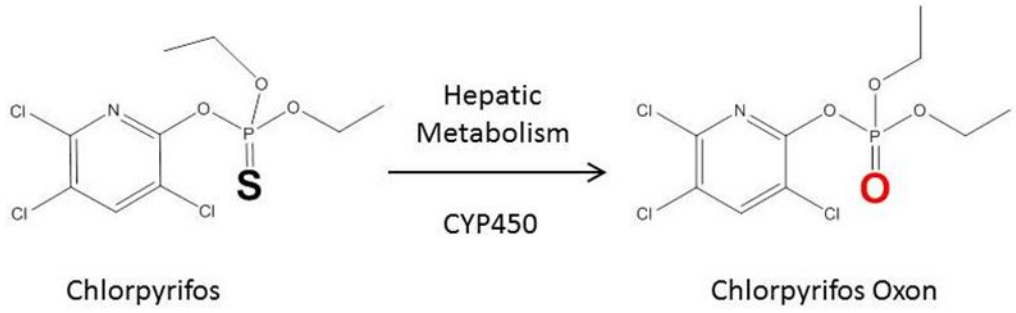

Figure 1. Bioactivation of chlorpyrifos to chlorpyrifos oxon.

The acute toxicity of OPs is associated with the inhibition of the enzyme acetylcholinesterase (AChE). Acetylcholinesterase is the enzyme responsible for the regulation of signaling between neurons and other cells mediated by the neurotransmitter, acetylcholine. Extensive AChE inhibition blocks acetylcholine inactivation at cholinergic synapses throughout the nervous system, leading to prolonged activation of cholinergic receptors and signs of cholinergic toxicity (10). Cholinergic toxicity is a result of excessive and prolonged activation of cholinergic receptors following AChE inhibition (11). Typical signs and symptoms of acute cholinergic toxicity include blurry vision, vomiting, diarrhea, convulsions, muscle twitching, and respiratory failure, the ultimate cause of death. Like other OPs, the "target" enzyme for acute CPF toxicity, is acetylcholinesterase (AChE). Alternative, non-cholinesterase macromolecular targets for

OPs have been the subject of investigation for decades, however, that could potentially participate in modulation of the toxicity of AChE inhibition as well as contribute to non-cholinergic toxicity pathways (12,13). For example, AChE is a serine hydrolase and a number of other serine hydrolases have been shown to be sensitive to inhibition by OPs (13,14). One other serine hydrolase that is sensitive to in vivo inhibition by CPF (as well as in vitro inhibition by CPO) is fatty acid amide hydrolase (15).

Fatty acid amide hydrolase (FAAH) is an important regulator of signaling pathways in a variety of physiological functions including sleep induction, analgesia, and energy homeostasis (16). Numerous studies have reported that FAAH is a secondary target of action of several OPs (17–19). CPO and other OPs inhibit FAAH via covalent binding to its active site serine residue within the catalytic triad, which is essentially the same mechanism by which CPO inhibits AChE (20). Of particular importance is that FAAH is the primary enzyme involved in the inactivation of the endocannabinoid anandamide (N-arachidonoylethanolamine, AEA) and the endocannabinoid-like metabolites, palmitoylethanolamide (PEA) and oleyoylethanolamide (OEA) (21).

Humans have been using cannabinoids for thousands of years for medical, religious, and (likely only relatively recently) recreational purposes. The cannabis plant (*C. sativa, C. indica*) contains a large number of cannabinoids including the psychotropic compound delta 9-tetrahydrocannabinol (THC) (22,23). The discovery of a specific G protein-coupled receptor, the cannabinoid CB1 receptor that bound with high affinity to THC in the late 1980s, and subsequent discovery of endogenous ligands initiated the characterization of the endogenous cannabinoid (endocannabinoid) signaling pathway (17,24). Since that time, another specific cannabinoid receptor (CB2) was identified and

interactions between the endocannabinoids and endocannabinoid-like metabolites with these and other receptors have been described. Together, these many studies have shown the role of endocannabinoids in modulation of nervous (primarily through CB1 receptors) and immune (primarily through CB2 receptors) function (25,26).

The endocannabinoid (eCB) system constitutes a global neuromodulatory network that regulates neurotransmitter release at neuron presynaptic terminals (27). The receptors (mainly CB1), along with endocannabinoids, and the enzymes responsible for both their biosynthesis and degradation, make up this pathway. Endocannabinoid signaling is important in a number of neurological functions including appetite regulation, pain perception, cognitive development, emotional state, seizures and many others (25,28). The eCB system also plays an important role in lipid homeostasis and energy balance. The two primary eCBs (AEA) and 2-arachidonoylglycerol (2-AG), are synthesized "on demand" from membrane phospholipids following neuronal depolarization (26,29). The eCB AEA and the eCB-like metabolites OEA and PEA are capable of binding to and activating peroxisome proliferator-activated receptors, potentially influencing the expression of their target genes (30).

Peroxisome proliferator-activated receptors (PPARs), which form a subfamily of the nuclear receptor superfamily, are ligand-regulated transcription factors linked to the regulation of genes involved in several pathways of lipid metabolism include fatty acid oxidation, lipid transport, lipogenesis, and cholesterol metabolism, making PPARs essential components of energy homeostasis (31,32). Although there are three identified PPAR isoforms (PPARα, PPARγ, and PPARβ/δ), for the current study we chose to focus on two: PPARα and PPARγ.

As a major regulator of metabolic functions in the liver, PPARα expression is high in hepatocytes, where it has important roles in fatty acid oxidation, triglyceride clearance, cholesterol homeostasis, and lipoprotein production (33). PPARγ is also expressed in liver tissue, although it is predominately located in adipose tissue, where it plays a major role in adipocyte differentiation (32,33). PPARγ-induced lipogenesis is not limited to fat cells. It also helps regulate which cells differentiate into myelin, which is essential for normal function of myelinated axons (32,33). In order for PPAR to regulate target gene expression, they first dimerize with the retinoid X receptor (RXR, another nuclear receptor) which subsequently binds to specific peroxisome proliferator response elements (PPREs) (34). The heterodimer formation with RXR requires binding of a PPAR agonist, which changes the conformation of the PPAR in a manner that allows for the heterodimerization to occur. AEA, PEA and OEA, are all PPAR agonists that can bind to PPARs, allowing the heterodimer formation and binding to the PPRE and leading to PPAR transcriptional activity. Figure 2 illustrates the heterodimer formation and binding to the PPRE.

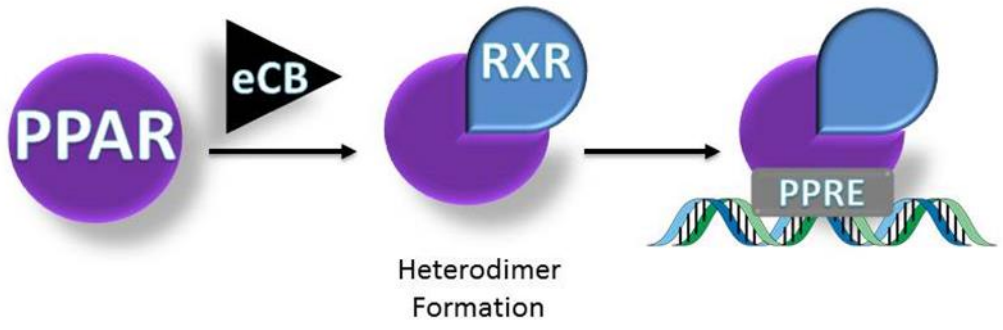

Figure 2. Endocannabinoid binding to PPAR alters the conformation, allowing for heterodimer formation with RXR, and subsequent PPRE binding to alter transcription of target genes.

In addition to concern over the adverse effects of OP pesticides, such as chlorpyrifos, in terms of its effects on cholinergic signaling, numerous other pathways of possible OP toxicity have been subjects of investigation for the last couple of decades (20,35). These studies include effects of pre-natal and juvenile exposure on neurological and cognitive development, as well as neurodegenterative diseases among other physiologic pathologies affecting older adults, and psychological disorders that effect behavior, learning, and response to stressors (36–38). Many investigations have suggested that adverse outcomes can be associated with levels of exposure below those which inhibit acetylcholinesterase (35,39). Furthermore, there is a growing concern for chronic effects on metabolic function that may lead to issues related to heart disease, diabetes, and obesity (5,40). Multiple studies have demonstrated that exposure to chlorpyrifos oxon causes weight gain in both juvenile and adult rats, as well as altered metabolic functions related to lipid homeostasis in prenatally exposed mice (12,39,41). The results of such studies suggest that exposure to environmental chemicals like OP pesticides are possible contributors to the ever increasing incidence of metabolic disorders in humans (5,42).

The obesity epidemic in the United States has continued to expand over the last several decades, affecting all age groups including young children, adolescents, and adults (43,44). Although inactivity, dietary habits, and genetic predisposition are all factors contributing to current trends, they are still not sufficiently enough to adequately explain the continuously increasing percentages of obesity throughout the population (42,45). It can be postulated that exposure to environmental chemicals is a possible contributing cause to the growing obesity epidemic considering that, in addition to acute

exposures, the population of the U.S. is exposed chronically to a wide variety of environmental chemicals that are used to protect food crops and commercial, residential, and industrial buildings from pest infestations (46). These chemicals include insecticides, such as chlorpyrifos. We hypothesized that exposure to OPs such as chlorpyrifos may lead to downstream changes in the expression of PPAR target genes involved in the regulation of lipid metabolism by inhibiting FAAH, increasing AEA and/or PEA and OEA which increases PPAR activation and alters lipid metabolism-related genes.

There are three important steps that help to define the processes involved in transcriptional regulation of lipid metabolism: 1) Upstream events that define the signaling, 2) molecular mechanisms that control the operation of transcription factors, and 3) downstream events that affect the target genes (47). Disruption of normal PPAR signaling can lead to a number of potentially adverse effects associated with dysregulated gene expression, including increased lipogenesis, insulin desensitization, dysfunctional cholesterol metabolism, faulty lipid transport mechanisms, and excess energy storage in the form of fat (48–50). The objective of this study was to evaluate the possible role of CPF as a contributing factor to altered metabolism and obesity. Although a number of studies have associated an OP exposure with increased body fat, and that show OPs such as chlorpyrifos can be potent inhibitors of FAAH, none have characterized potential changes in PPAR signaling as a consequence of the OP induced inhibition of FAAH, creating a direct link between exposure to organophosphorus pesticides and obesity.

To evaluate CPO's effect on FAAH and PPAR signaling, we compared the *in vitro* concentration-dependent effects of CPO on FAAH and AChE activity, as well as on PPAR signaling in the MCF-7 human breast cancer cell line. This cell line was chosen

based on species relevance for extrapolation, the presence of both "target enzymes", the presence of both PPAR subtypes, as well as functional PPAR signaling pathways (51). Four genes that are regulated by PPARs were selected based on their role in the regulation of lipid metabolism, and for their known expression in the MCF-7 cell line (51).

The liver X receptor alpha (LXRα), like the PPARs, is also a member of the nuclear receptor superfamily, and is a transcription factor involved in the regulation of genes responsible for multiple cellular functions associated with nutritional regulation and lipid metabolism (52). As a key regulator of hepatic cholesterol metabolism, LXRα is predominantly expressed in the liver, but is also expressed in adipose tissue, spleen, kidneys, macrophages, and the small intestine, where it serves as a primary regulator of intestinal cholesterol absorption (52). Interestingly, LXRα shares RXR as an obligate heterodimer partner with PPARs, and it has been demonstrated that LXRα and PPARα have a unique dynamic in their interaction as reciprocal regulators of nutritional fatty acid metabolism (53). Although LXRα was chosen primarily as a target for PPARα, it has been recently found that its expression is also regulated by PPARγ (53). Acyl-CoA oxidase (ACOX) was also selected as a target gene of PPARα. Human ACOX1 is highly expressed in the liver, as well as skeletal muscle and the kidneys. It is the first, and rate limiting, enzyme in the fatty acid β-oxidation pathway (54,55).

The genes selected in which expression is primarily regulated by PPARγ were 1-acylglycerol-3-phosphate-*O*-acyltransferase (AGPAT2), and a member of the ATP-binding cassette transporter super family, ABCG2. AGPAT2 belongs to the enzyme family of acyltransferases, and plays an important role in the biosynthetic pathway for

triaglycerols and glycerophospholipids (56,57). It is expressed primarily in adipose tissue, but is also found in the liver and pancreas. In fact, ABCG2 was originally identified as an overexpressed protein in the MCF-7 cell line (58). ABCG2 is expressed ubiquitously, but is most abundant in the liver, intestines, central nervous system, and the placenta. Substrates for ABCG2 include a wide variety of both endogenous and exogenous compounds (58,59). It is the ability of ABCG2 to transport such a diverse range of substrates that makes it a critical component of xenobiotic metabolism, as it plays a protective role against absorption of toxicants in barrier tissues, and facilitates clearance in organs such as the liver (59).

The specific aims of this study were as follows:

1. Measure the amount of FAAH inhibition by CPO.

2. Determine concentration dependent effects of CPO inhibited FAAH on exogenous agonists.

3. Assess changes in expression of PPARα and PPARγ target genes in cells exposed to the concentrations of CPO, and exogenous agonists co-administered with those concentrations of CPO.

CHAPTER II

METHODS

Chemicals and Reagents

Eagle's Minimum Essential Medium and fetal bovine serum were purchased from Quality Biological Inc. Chlorpyrifos oxon (CPO, >97% purity) was purchased from Chem Service and kept desiccated under nitrogen at -70C. The desiccator containing CPO was brought to room temperature under the fume hood before opening to minimize any CPO hydrolysis. Eagle's Minimum Essential Medium, fetal bovine serum, and DMSO were all purchased from ATCC. 5- amino-2-methoxypyridine was purchased from Sigma-Aldrich. Octanoyl methoxypyridine and was a kind gift from Dr. Bruce Hammock, UC Davis. TaqMan gene expression assays, TaqMan Fast Advanced Master Mix No AMP Erase UNG, and the High Capacity cDNA Reverse Transcription Kit were all purchased from Applied Biosystems. Anandamide and oleyoyl ethanolamide were both purchased from Cayman Chemical. Pioglitazone was obtained from Adipogen, and clofibrate was purchased from Thermo Fisher Scientific Chemicals, Inc.

Cell Culture

Human MCF-7 cells were obtained from American Type Culture Collection (ATCC, HTB-22). Cells were initially seeded in 25 cm^2 flasks, and sub-cultured at a ratio of 1:3 once a confluency of ~90% was reached. Cultures for chemical exposure, or assay use, were seeded at a density of ~ 4.2 x 10^6 cells per 60 mm plate in 4 mL complete culture medium (Eagle's Minimum Essential Medium, 10% FBS, insulin (human recombinant) 0.01 mg/mL). Cells were incubated at 37°C in 5% CO2 until they formed an adherent layer (generally 24-36 hours). Prior to any treatments, plates were removed from the incubator and the medium was aspirated before any chemical exposures. All chemicals were provided in fresh complete medium.

Enzyme Assays

Sample Collection and Preparation

The sample collection and preparation was performed the same way for all enzyme assays. At each time for collection, plates were removed from the incubator, medium aspirated, and the cells were rinsed three times with 1 mL ice-cold PBS. Lysates were made by adding 0.5 mL ice-cold lysis buffer (1 mL 50 mM EDTA, 25 mL 50 mM Tris HCl pH 7.4, 50 uL Triton X-100, 7.5 mL 1 M NaCl, and deionized water added to 50 ml final volume) to each plate, followed by incubation on a bed of ice for 10 minutes. A cell scraper was used to detach any remaining, adherent cells and each lysate was transferred to a pre-chilled culture tube on ice. Each lysate was kept on ice and homogenized for 30 seconds using an Eberbach Con-Torque tissue homogenizer, then

transferred to pre-chilled Eppendorf tube (1.5 ml). Tubes were then centrifuged at 12,000 x g for 15 minutes at 4°C. The supernatant was removed and transferred to a clean pre-chilled Eppendorf tube and the pellet discarded. The supernatants were kept at -80°C until use.

Total Protein Quantitation

Prior to performing any enzyme inhibition assays, it was necessary to measure the activities of AChE and FAAH in cell lysate over a range of protein concentrations. The supernatants collected, as described above, were thawed on ice. Serial dilutions of the cell lysate were made using the lysis buffer. Total protein for each dilution was quantified using the method described by Bradford (60). A standard curve was created using bovine serum albumin (BSA) (Sigma) diluted in the lysis buffer for a range of concentrations from 0.14 mg/mL to 1.14 mg/mL protein. Lysis buffer was used in the plate blank wells. Each well contained 4 uL of sample (or buffer for blanks) and 200 uL Bradford Reagent (Sigma) for a total reaction volume of 204 uL per well. All blanks and sample dilutions were loaded as quadruplicate replicates. The plate was incubated in the drawer, away from light, for 10 minutes prior to reading. Absorbance at 595 nM was read using a SpectraMax 340PC plate reader (Molecular Devices). The average optical density (OD) for each sample dilution was then compared to that of the BSA standard curve and the mg/mL protein interpolated using GraphPad Prism 6.

Enzyme Activity

AChE activity was measured using a method similar to that described by Ellman (61). Plates were prepared on ice by first adding 25 uL of sample dilution to wells, in

replicates of 4. Lysis buffer was used for plate blank wells. A DTNB-substrate cocktail (10 mM Tris buffer pH 7.2, 1 mM EDTA, 7.62 mM acetylthiolcholine, 1.086 mM DTNB) was mixed shortly before loading into the plate. Each well contained 175 uL of the DTNB-substrate cocktail for a total reaction volume of 200 uL. Once loaded, the plates were immediately placed into the SpectraMax 340PC plate reader. Activity was measured kinetically at 412 nM, reading once every 60 seconds for 10 minutes.

FAAH activity was measured by following a fluorometric method described by Huang et al. (15). A 10 mM stock solution of the substrate octanoyl methoxypyridine (OMP), to produce a final concentration of 500 uM in the plate wells, was prepared in advance by dissolving the OMP in a 1:1 mixture of DMSO/EtOH. The substrate solution was kept stored at 4^{o} C, away from light. Black, 96-well fluorometric plates were prepared on ice. Sample wells contained 30 uL of cell lysate and the plate blank wells contained 30 uL lysis buffer in place of the cell lysate. A range of concentrations 100 nM to 5000 nM of 5-amino-2-methoxypyridine (AMP) was used to generate a standard curve within each plate run. Samples were put in the plates as replicates of 4, AMP standards were loaded as duplicates. Plate blank and AMP standard wells contained 10 uL of 1:1 DMSO/EtOH in place of the OMP substrate. Assay buffer, a solution of 125 mM sodium phosphate, pH 8, 1% glycerol, 0.1% Triton X – 100, was added to all wells for a total reaction volume of 200 uL. The OMP/EtOH/DMSO (10 uL) was added to the sample-containing wells immediately before loading the plates into a BMG Labtech CLARIOstar plate reader. Plates were read for 10 minutes, with fluorescence (excitation: 320 nM, emission: 396 nM) measured every 60 seconds, and results given in terms of relative fluorescence units (RFUs), based on the hydrolysis of OMP to AMP.

Enzyme Inhibition Assays – Supernatant Treated

For initial measurements of AChE and FAAH inhibition, cells were collected and samples prepared as described above. The supernatants were thawed on ice, then incubated for 20 minutes in a 37^{o} C water bath, with shaking, with various concentrations of chlorpyrifos oxon diluted in Tris-E, 1% EtOH. Concentrations used were 5 nM, 10 nM, 30 nM, 50 nM, 100 nM, 500 nM, and 1 uM. For the control sample, cell lysate was incubated with Tris-E, 1% EtOH. Activities were measured then using the same methods as described above for the respective enzyme. Additional FAAH inhibition assays were performed under the same conditions, using the same methods, but by adding complete culture medium to the incubation mixtures, to investigate whether, or not, the fetal bovine serum in the culture medium would interfere with CPO's ability to inhibit FAAH. The results from the FAAH inhibition assays that included complete culture medium were used to decide which concentrations of CPO would be used to treat cell cultures for the measurement of gene expression changes.

Enzyme Inhibition Assays - Cells Treated in Culture

The treatment method for enzyme inhibition using cells exposed while in culture was the same for both AChE and FAAH assays. Once ready for treatment, cells were removed from the incubator, medium aspirated. Cultures were given fresh complete medium containing CPO at concentrations of 250 nM, 500 nM, 1 uM, 2 uM, 3 uM, or 5 uM in DMSO. Vehicle only treated cells (control) were given complete medium with a 1% DMSO concentration, and all CPO treated plates also had a final DMSO concentration of 1% in the medium. Cells were collected at 8 hours, 1 day, and 3 days

post-exposure using the cell collection and sample preparation methods described above. Enzyme activities for AChE and FAAH were then measured using the respective methods as described above, as well.

Quantitative Reverse Transcription Polymerase Chain Reaction (RT-qPCR)

Treatments for measurement of gene expression changes were as follows: vehicle only (DMSO) for reference control samples, 250 nM CPO, 500 nM CPO, 1 uM CPO, OEA, AEA, OEA + 250 nM CPO, OEA + 500 nM CPO, OEA + 1 uM CPO, AEA + 250 nM CPO, AEA + 500 nM CPO, AEA + 1 uM CPO. Clofibrate and pioglitazone were used for positive controls as agonists at PPARα and PPARγ, respectively. All had a final DMSO concentration of 1%. Cells were exposed for 8 hours, 1 day, or 3 days.

RNA Isolation

At the post-exposure collection times, culture plates were removed from the incubator, and medium was aspirated. 1 mL Trizol reagent (Invitrogen) was added to each plate to lyse the cells. The mixture was homogenized in the plate by pipetting up and down three times before being transferred to a 1.5 mL Eppendorf tube. Tubes containing the cells in Trizol were left to incubate 5 minutes at room temperature, to allow time for complete dissociation of the nucleoproteins. 200 uL of chloroform was then added to each tube. Tubes were vigorously vortexed for 15 seconds, then incubated at room temperature for 3 minutes. Samples were then centrifuged for 15 minutes at 12,000 x g, 4^{o} C. After centrifugation, the aqueous phase was removed and transferred to a fresh 1.5 mL Eppendorf tube, the rest was discarded. To precipitate the RNA, 500 uL isopropanol was added to each tube and mixed by inversion. The tubes were incubated at room

temperature for 10 minutes prior to centrifugation at 12,000 x g, 4° C for 10 minutes. The supernatant was then removed from each tube, and pellets were washed by adding 1 mL 75% ethanol to each tube, vortexed gently, then centrifuged again for 5 minutes at 7500 x g, 4° C. After washing, ethanol was removed from the tubes and pellets were air dried for 10-15 minutes. Each pellet was re-suspended in 20 uL RNase-free water, then incubated for 15 minutes on a heat block set to 60° C. Total RNA was quantified by the absorbance method (A260/A280 ratio) using a Beckman Coulter DU530 UV/Vis spectrophotometer. RNA samples were stored at -70° C until used for cDNA synthesis.

cDNA Synthesis

RNA samples were removed from the -70° C freezer and thawed on ice. Applied Biosystems High Capacity cDNA Reverse Transcription Kit was used for cDNA synthesis. Kit components were thawed on ice, then mixed according to the manufacturer's protocol. Reactions were carried out in 0.5 mL RNase-free tubes. Tubes were prepared on ice by adding 10 uL of the reverse transcription master mix to 10 uL of RNA template, for a total reaction volume of 20 uL in each tube. Contents were mixed by pipetting before tubes were sealed. Tubes were centrifuged for 4 minutes at 2500 x g, 4° C before being placed into the thermal cycler (Eppendorf Mastercycler Gradient). The thermal cycling conditions were set at 25° C for 10 minutes, 37° C for 120 minutes, 85° C for 5 minutes, 4° C for 120 minutes. After completion of the thermal cycling protocol, cDNA samples were stored at -20° C until ready to use for RT-qPCR.

RT-qPCR

RT-qPCR reactions were carried out in an Applied Biosystems 7500-Fast Real Time PCR System. Thermal protocol settings, as specified by the manufacturer for TaqMan Fast Advanced Master Mix, were UNG incubation 50° C for 2 minutes (1 cycle), enzyme activation 95° C for 20 seconds (1 cycle), denature 95° C 3 seconds (40 cycles), and anneal/extend 60° C for 30 seconds (40 cycles). Experiments were set up in the system software as comparative Ct, using the vehicle treated samples as reference, and β-Actin as the endogenous control. Plate layouts were entered prior to preparation. Each sample type and target gene for each sample type was run as triplicates. No treatment controls (NTCs) for blanks contained nuclease-free water in place of cDNA. The dyes in each reaction mix were FAM (reporter), NFQ-MGB (quencher), and ROX (passive reference). Reactions were set as two-step, singleplex.

Prior to plate preparation, all equipment and surfaces were cleaned with RNase-Zap wipes. The TaqMan assay tubes containing the primers and probes for each target gene, and the cDNA samples were all thawed on ice. Primer sequences are listed in Table 1. The primer/probe tubes were kept covered to protect from light while thawing. Reaction mixes were prepared according to the manufacturer's protocol for TaqMan gene expression assays, then loaded into 96-well fast optical plate, with a final reaction volume of 20 uL in each well. The plates were kept on a cold block while loading samples and reaction mixes into the wells. Once loaded, the plates were sealed with optical adhesive film, then centrifuged for 4 minutes at 2500 x g, 4° C to remove bubbles and ensure that all contents were at the bottom of the wells. After centrifugation, plates were immediately placed into the PCR machine, and run started.

Gene Symbol	NCBI RefSeq	Primer (5' – 3')
β-Actin	NM_001101.3	CCCAGGCACCAGGGCGTGATGGTGG
LXRα (NR1H3)	NM_001130101.2	TTTGCCAAAGCAGGGCTGCAAGTGG
ABCG2	NM_001257386.1	GGAGGCAAATCTTCGTTATTAGATG
ACOX1	NM_001185039.1	AGCAGAGGTCCACGAATCTTACAAG
AGPAT2	NM_001012727.1	GGTGGAGAACATGAGCATCATCGGC

Table 1. TaqMan® gene expression assays for RT-qPCR. β-Actin used as the endogenous control reference gene.

Data Analysis

All enzyme activities were calculated in terms of nmol/min/mg protein, and inhibition rates expressed as percent activity compared to the vehicle only control. Results from independent replicate assays were grouped and graphed using GraphPad 6 software. PCR results were analyzed using the ΔΔCt method. Ct values below 16 and above 35 were removed from the results before any further calculations or analysis. Gene expression changes were normalized against the reference gene β-actin and are presented as relative fold change over vehicle control samples, all of which were complete culture medium with a 1% concentration of DMSO. Relative fold changes in gene expression were calculated using Microsoft Excel as $2^{-\Delta\Delta Ct}$ for each target gene as follows:

ΔCt = Ct β-actin – Ct target

$\Delta\Delta Ct$ = ΔCt treatment – mean ΔCt vehicle control

Relative fold change = $2^{-\Delta\Delta Ct}$

Results for each gene were grouped into related treatments for each of the three time points. Further statistical analyses were performed on each group using GraphPad Prism 6 software by subjecting the data to a two-way ANOVA, followed by Tukey's multiple comparisons test. The two-way ANOVAs were done to detect significant effects on gene expression changes based on treatment and exposure time. The Tukey's multiple comparisons tests were carried out to compare the means of each treatment group within each time point.

CHAPTER III

RESULTS

Enzyme Assays

The initial assays to quantify AChE and FAAH activity in various dilutions of cell supernatant demonstrated a protein concentration-dependent effect on the rates of hydrolysis for their respective substrates. Interestingly, the results from the data showed the activity rate of AChE as lower than that of FAAH in the cell supernatant samples, which is the opposite of what would typically be expected. Based on the results from inhibition assays performed by incubating cell supernatant with various concentrations of CPO prior to the assay, the most appropriate concentrations of CPO to use in treatment of cells for measurement of gene expression changes were determined to be 250 nM, 500 nM, and 1 uM. Although the enzyme activity rates that were determined initially based on total protein concentrations in the absence of an inhibitor showed that FAAH activity was higher compared that of AChE in samples of similar protein content, the sensitivities to CPO inhibition were much more closely related in the corresponding CPO concentrations. Analysis of inhibition over time was necessary to ensure that FAAH was still being inhibited in the cells after such duration of exposure in culture to the same concentrations of CPO used to assess changes in target gene expression, and to

investigate the possible existence of any relationships between the levels of FAAH inhibition and expression of the target genes.

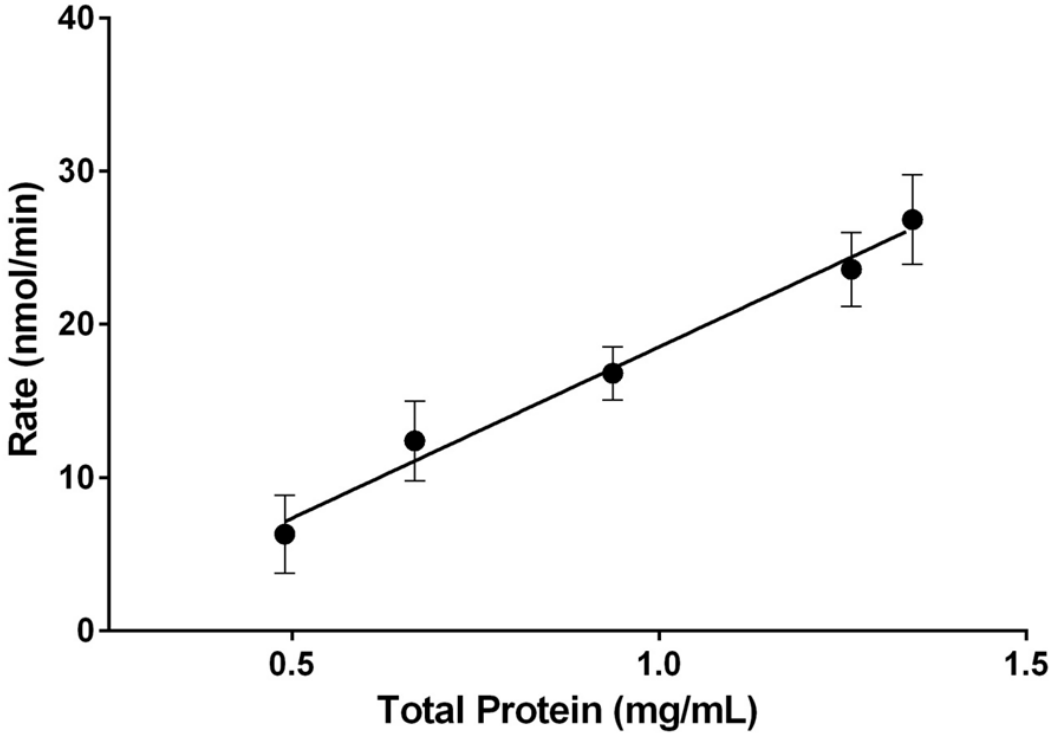

Figure 3. Protein concentration-dependent rates of OMP hydrolysis to AMP. Supernatant dilutions were collected and total protein quantified as described in methods. Data are reported as mean ± SEM, n = 4. Linear regression analysis determined the rate of hydrolysis was highly correlated with protein concentration ($p = 0.0006$, $r^2 = 0.99$).

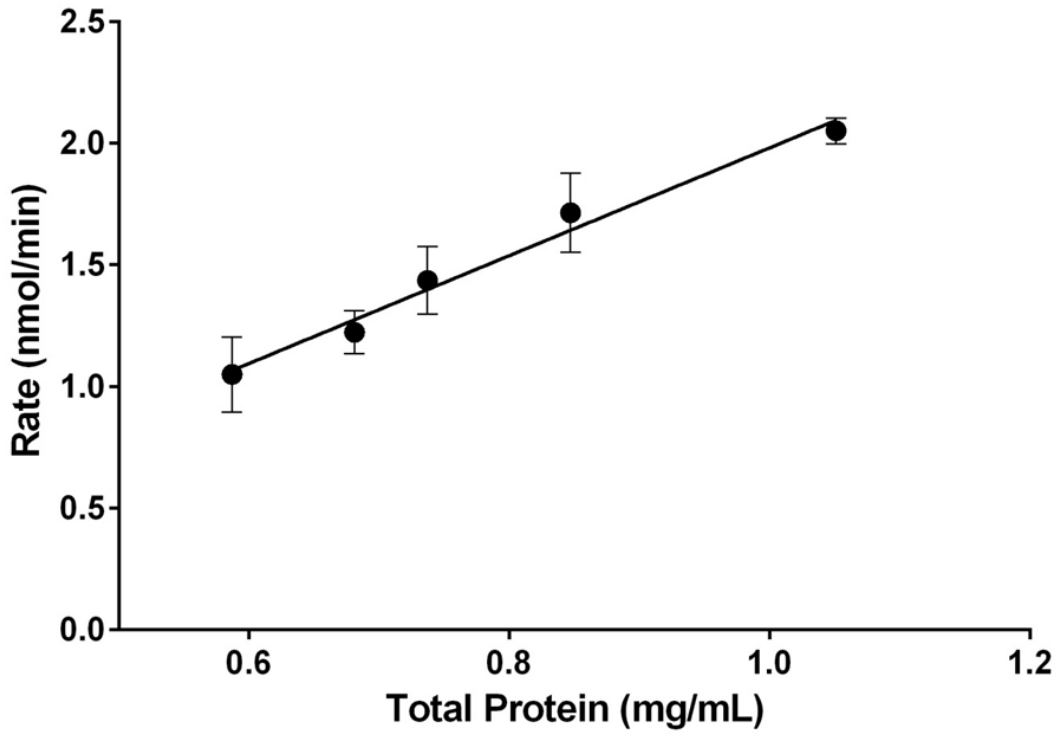

Figure 4. Protein concentration-dependent rates of AChE hydrolysis of acetylthiocholine. Dilutions were made of the cell supernatant collected and total protein was quantified as described in methods. Data are shown as mean ± SEM, n = 4. Linear regression analysis determined the rate of hydrolysis was highly correlated with protein concentration ($p = 0.001$, $r^2 = 0.98$).

Data from figures 3 and 4 allowed selection of assay conditions for subsequent assays to achieve linear rates of hydrolysis for FAAH and AChE, respectively.

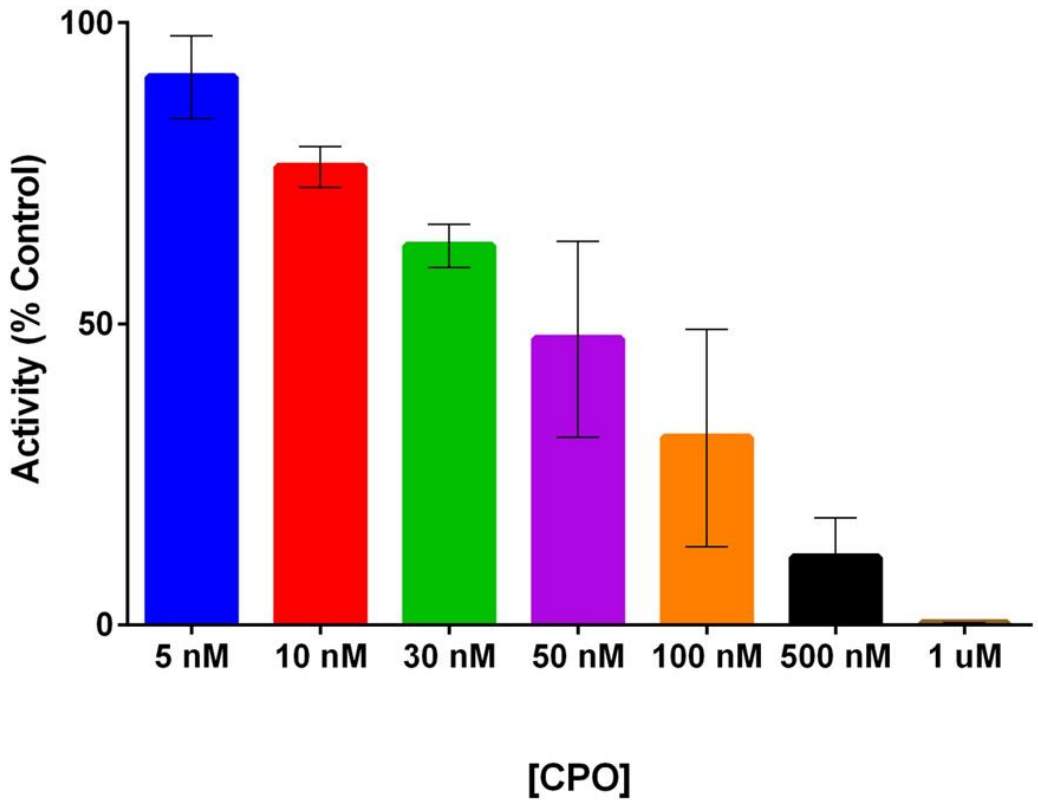

Figure 5. Inhibition of FAAH in cell supernatants. The supernatant, collected as described in methods, was incubated at 37° C with a range of concentrations of chlorpyrifos oxon for 20 minutes prior to assay of residual activity at 37° C. Data are expressed as mean (± SEM of the percent of control activity, n = 4 independent assays).

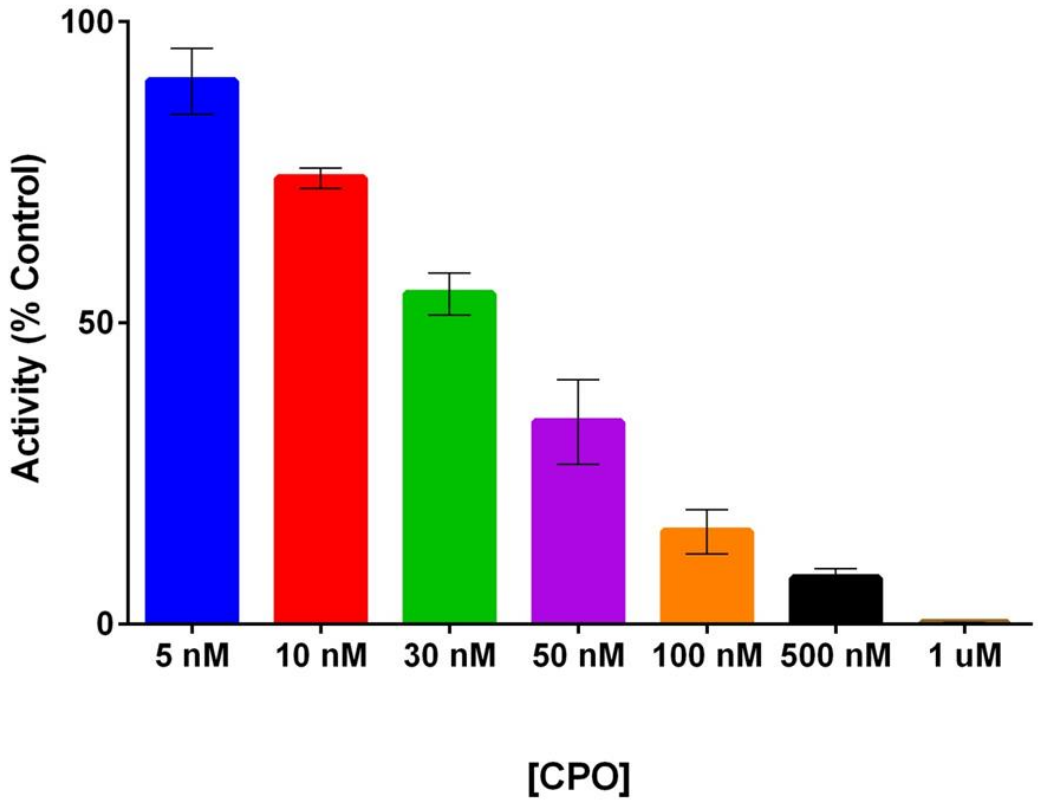

Figure 6. Inhibition of AChE in cell supernatants. The supernatant, collected as described in methods, was incubated at 37° C with a range of concentrations of chlorpyrifos oxon for 20 minutes prior to assay of residual activity at 37° C. Data are expressed as mean (± SEM of the percent of control activity, n = 3 independent assays).

The *in vitro* inhibition data presented in figures 5 and 6 suggest that both FAAH and AChE would be markedly inhibited by CPO at concentrations higher than 100 nM. These data allowed selection of CPO concentrations for in culture exposures (250, 500, and 1000 nM).

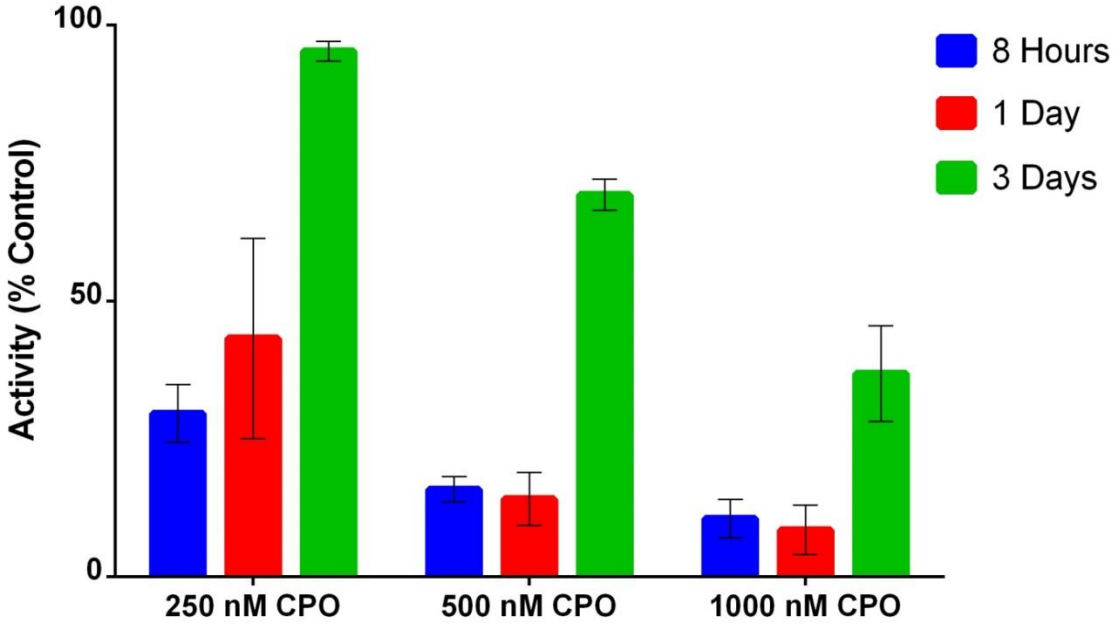

Figure 7. FAAH inhibition in cells exposed while in culture. Data expressed as mean ± SEM of the percent of control activity (n = 3).

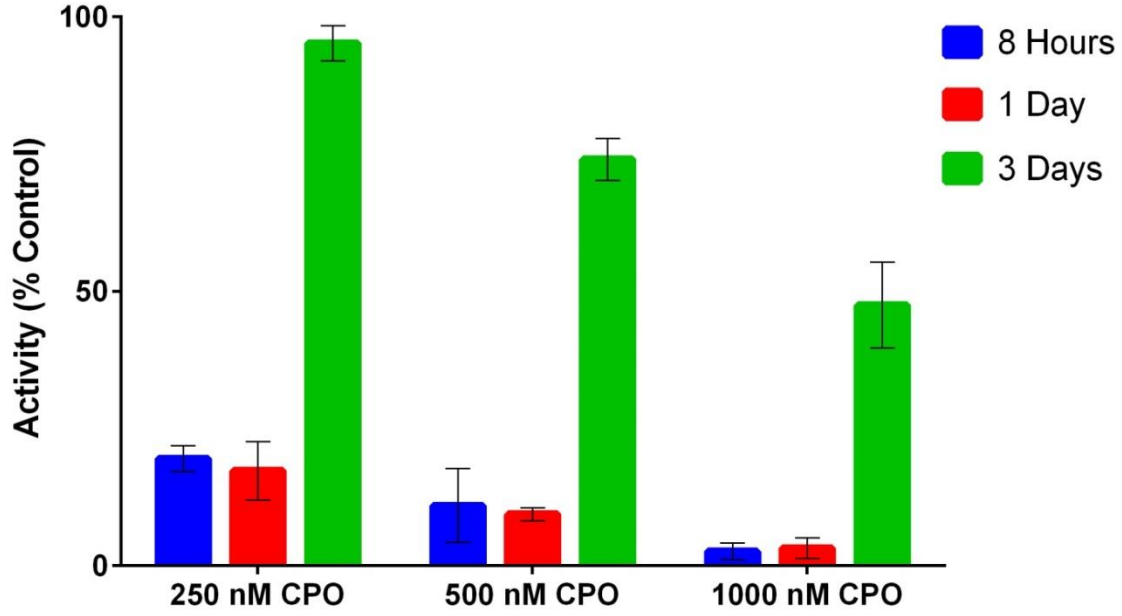

Figure 8. AChE inhibition in cells exposed while in culture. Data expressed as mean ± SEM of the percent of control activity (n = 3).

As shown in figures 7 and 8, both FAAH and AChE were inhibited by CPO at the concentrations selected. Moreover, more extensive inhibition of both enzymes was with the highest concentration at the earlier time points (8 hours and 1 day). By 3 days of exposure, substantial recovery was noted with both FAAH and AChE.

Gene Expression

We selected three concentrations of CPO eliciting concentration-related increasing FAAH inhibition to study effects on expression of representative genes regulated by PPARα and PPARγ. An exogenous ligand (AEA or OEA) was added to evaluate the interactive effects of CPO and the exogenous PPAR activator on gene expression. The following figures show concentration and time-dependent effects of CPO on expression of LXRα, ACOX1, AGPAT2, and ABCG2.

LXRα

Figure 9 shows the effects of CPO alone on LXRα expression after 8 hours, 1 day, and 3 days of exposure in culture. There was a significant main effect of both CPO ($F_{4,18}$ = 606, $p < 0.001$) and time ($F_{2,18}$ = 79, $p < 0.001$), as well as a significant interaction ($F_{4,18}$ = 112, $p < 0.001$). Pairwise comparisons across concentrations indicated significant differences within each time point for cells treated with CPO. In general, there was a step-wise, concentration-dependent increase after 8 hours, 1 day, and 3 days of exposure, and a significant increase with 1,000 nM CPO at all three time-points.

Figure 10 shows the effects of AEA (3 μM) alone or in the presence of CPO on LXRα expression. There was a significant main effect of treatment ($F_{3,24}$ = 13.35, $p < 0.0001$) and time ($F_{2,24}$ = 33.49, $p < 0.0001$), as well as a significant interaction ($F_{6,24}$ = 8.846, $p < 0.0001$). AEA increased LXRa expression (4.5-6 fold) after 24 and 72 hours of exposure. Pairwise comparisons indicated significant differences between AEA alone and AEA in the presence of 250 and 1,000 nM CPO as well as AEA in the presence of 1000 nM CPO compared to the lower CPO concentrations after 24 hours exposure.

Finally, in the exogenous agonist OEA alone or OEA plus CPO, there was a significant main effect of the treatments ($F_{3,24} = 42.04$; $p < 0.0001$), and time ($F_{2,24} = 11.35$; $p = 0.0003$), as well as a significant interaction ($F_{6,24} = 11.35$; $p < 0.0001$). OEA alone, as well as in the presence of CPO, had relatively little effect at any time point except with the highest concentration of CPO. In that case, the greatest increases (5-10 fold) were noted at 8 hours and 1 day, respectively.

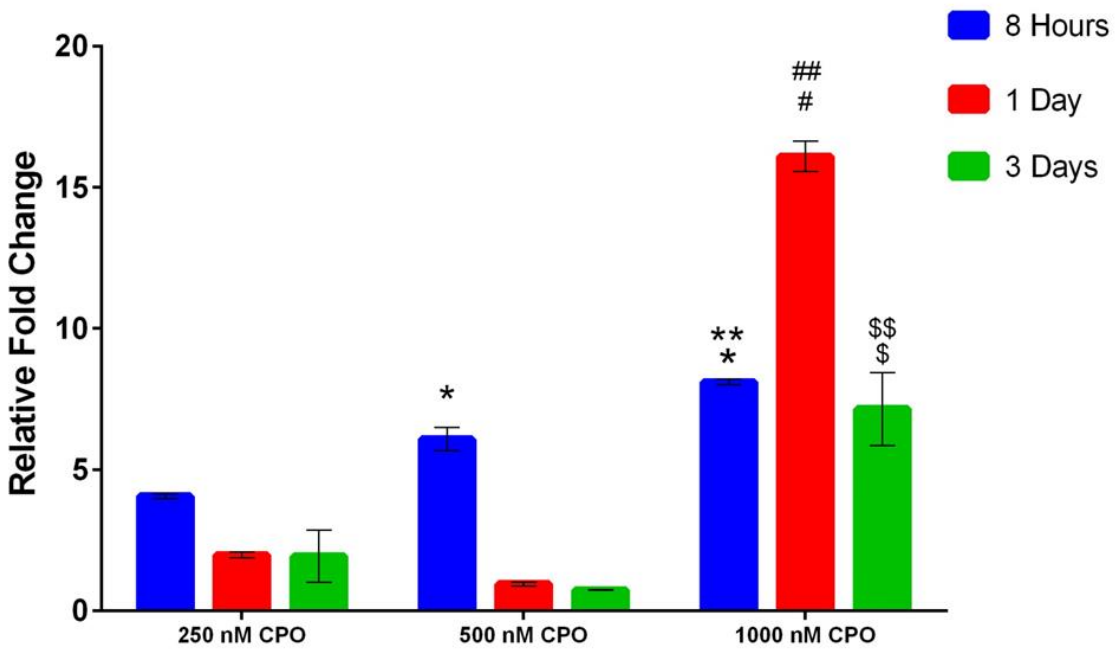

Figure 9. Effects CPO alone on LXRα expression. Relative fold change in expression of LXRα over vehicle control after exposure to CPO are shown. Data are presented as mean ± SD. At 8 hours after dosing, a single asterisk indicates a significant difference compared to 250 nM whereas a double asterisk indicates a difference compared to 500 nM CPO. At 1 day after dosing, a pound sign indicates a significant difference compared to 250 nM while a double pound sign indicates a difference from 500 nM CPO. At 3 days, a single dollar sign indicates a significant difference compared to 250 nM whereas a double dollar sign indicates a difference compared to 500 nM CPO.

In general, CPO elicited a concentration-and time-dependent increase in LXRα expression. At 8 hours, a step-wise concentration-dependent increase was noted while at 1 and 3 days, lower fold increases were noted except with the highest concentration. Thus, the changes noted at 8 hours suggested that this time may be best for evaluating concentration-dependent effects of CPO on expression of LXRα.

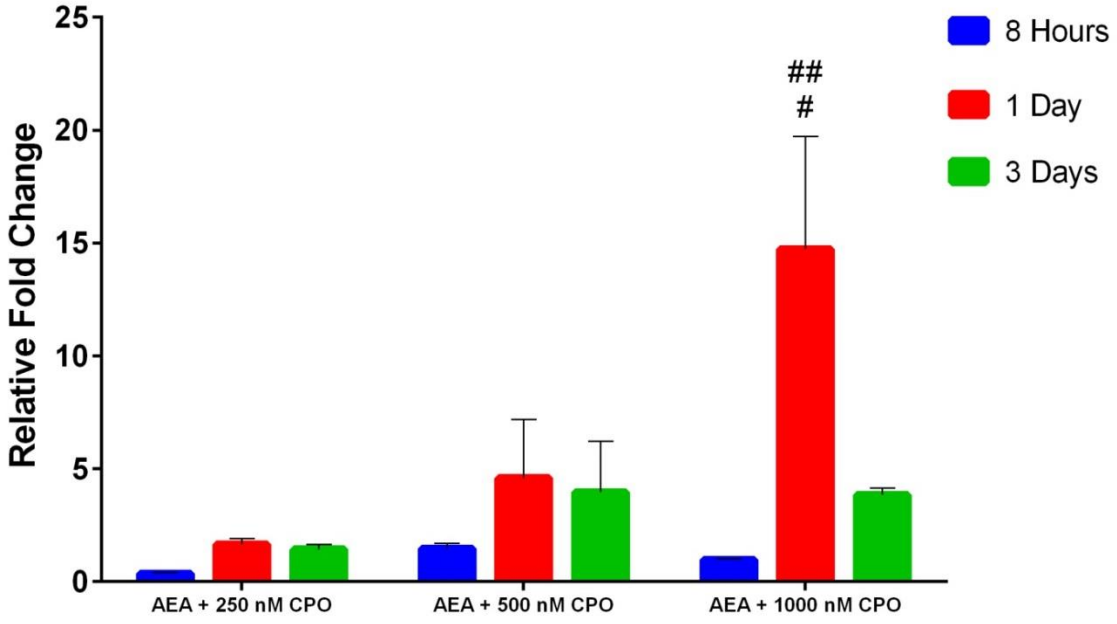

Figure 10. Effects of CPO in the presence of AEA on LXRα expression. Relative fold change in expression of LXRα over vehicle control after exposure to AEA in the presence of CPO is shown. Data represent mean ± SD. At 1 day after dosing, a pound sign indicates a significant difference compared to 250 nM, and a double pound sign indicates a difference compared to 500 nM.

AEA alone increased LXRα expression about 6-fold at the 1 day time-point. In the presence of 250 nM CPO however, no significant increase was noted at 1 day, or the other time-points. With the highest CPO concentration, the greatest fold increase was also noted at 1 day.

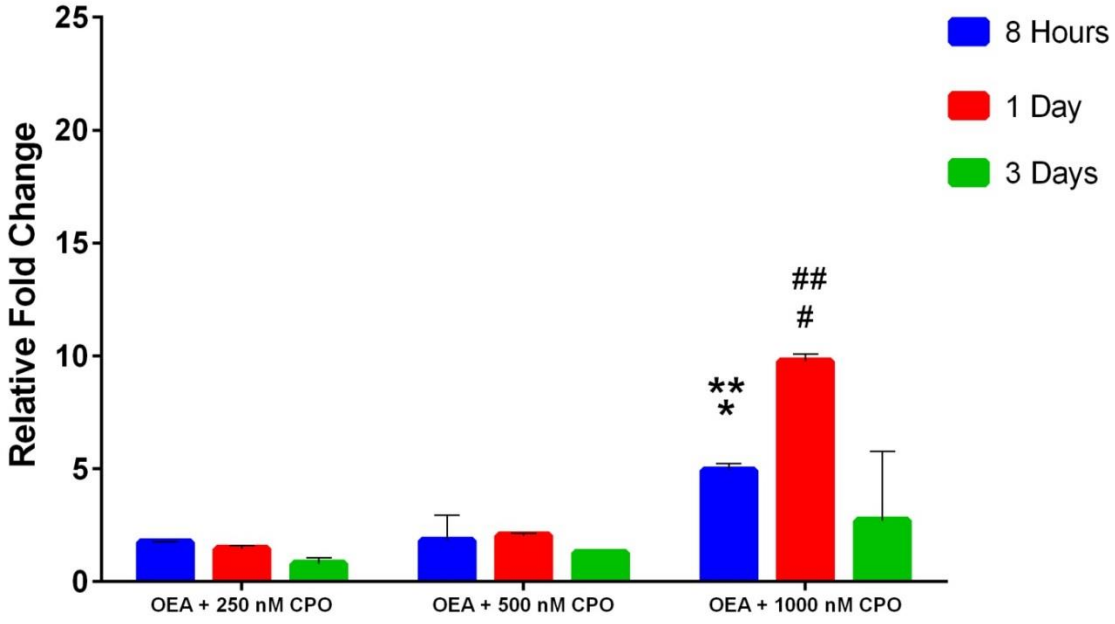

Figure 11. Effects of CPO in the presence of OEA on LXRα expression. Data are presented as mean ± SD. A single asterisk at the 8 hour time point indicates a significant difference compared to 250 nM whereas a double asterisk indicates a significant difference compared to 500 nM, and a triple asterisk indicates a difference from OEA combined with 1000 nM CPO. At 1 day after dosing, a pound sign indicates a significant difference compared to 250 nM while a double pound sign indicates a difference compared to 500 nM.

Similar to results evaluating the interactive effects of AEA and CPO, OEA had differential effects on LXRα expression when CPO was included. This interaction appeared blocked when the highest CPO concentration was used. Again, the greatest increase in LXRα expression was noted with the 1 day time-point and 1000 nM CPO.

	8 Hours	**1Day**	**3 Days**
AEA	0.12 ± 0.01	5.81 ± 0.35	4.15 ± 1.20
OEA	2.48 ± 0.39	1.11 ± 0.02	2.10 ± 0.05

Table 2. Effects of exogenous agonists AEA and OEA on LXRα expression in MCF-7 cells. Data are presented as mean relative fold change over vehicle only control, ± SD, n = 3.

ACOX1

Figure 12 shows the effects of CPO alone on expression of ACOX1, another gene under the control of PPARα. There was a significant main effect of both CPO ($F_{2,18}$ = 975.9, $p < 0.0001$), and time ($F_{2,18} = 1102.0$, $p < 0.0001$), as well as a significant interaction ($F_{4,18} = 345.2$, $p < 0.0001$). In general, CPO caused marked increases in ACOX1 expression, with the most substantial effects being noted at the earliest time-point (up to 55-fold with 1000 nM CPO). Pairwise comparisons across CPO concentrations indicated significant differences within each time- point.

We also evaluated the effects of the exogenous ligand AEA, in the presence and absence of CPO, on ACOX1 expression. AEA is a PPAR gamma agonist. Again, a main effect of treatment ($F_{3,24} = 117.9$, $p < 0.0001$), and time ($F_{2,24} = 67.96$, $p < 0.0001$) was noted, as well as a significant interaction ($F_{6,24} = 67.96$, $p < 0.0001$). A time-dependent increase in ACOX1 expression was noted with AEA alone at 1-3 days of exposure (4-8 fold). Pairwise comparisons across all treatments indicated significant differences within each time point. CPO (500 and 1000 nM) increased ACOX1 expression relative to AEA alone at 24 hours of exposure.

Figure 14 shows the effects of OEA in the presence or absence of CPO on ACOX1 expression. OEA is a selective PPARα agonist, so little effect was expected. There was a significant main effect of treatment ($F_{3,24} = 1747.0$, $p < 0.0001$) and time ($F_{2,24} = 140.5$, $p < 0.0001$), however as well as a significant interaction ($F_{6,24} = 199.9$, $p < 0.0001$). OEA alone did elicit relatively minimal increases (2-3 fold) at all three time-

points. Pairwise comparisons suggested significant differences between OEA alone and OEA in presence of the highest concentration of CPO.

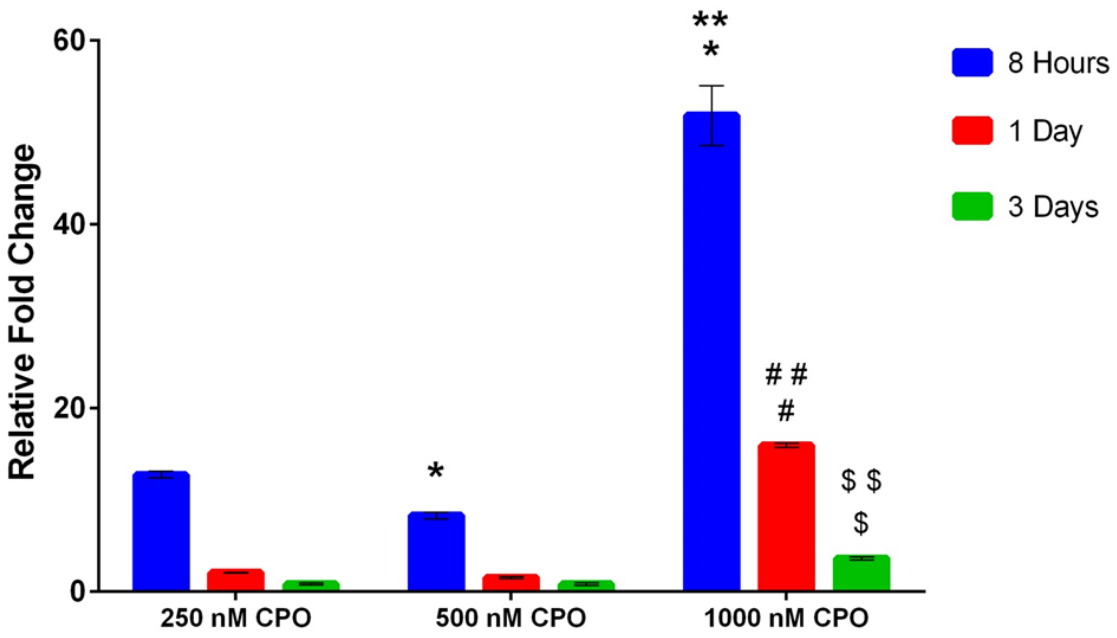

Figure 12. Effects of CPO on ACOX1 expression. Data are presented as mean relative fold change ± SD. At 8 hours after dosing, a single asterisk indicates a significant difference compared to 250 nM whereas a double asterisk indicates a difference from 500 nM CPO. At 1 day after dosing, a pound sign indicates a significant difference compared to 250 nM while a double pound sign indicates a difference compared to 500 nM. Finally at 3 days after dosing, a dollar sign indicates a difference compared to 250 nM whereas a double dollar sign indicates a difference compared to 500 nM CPO.

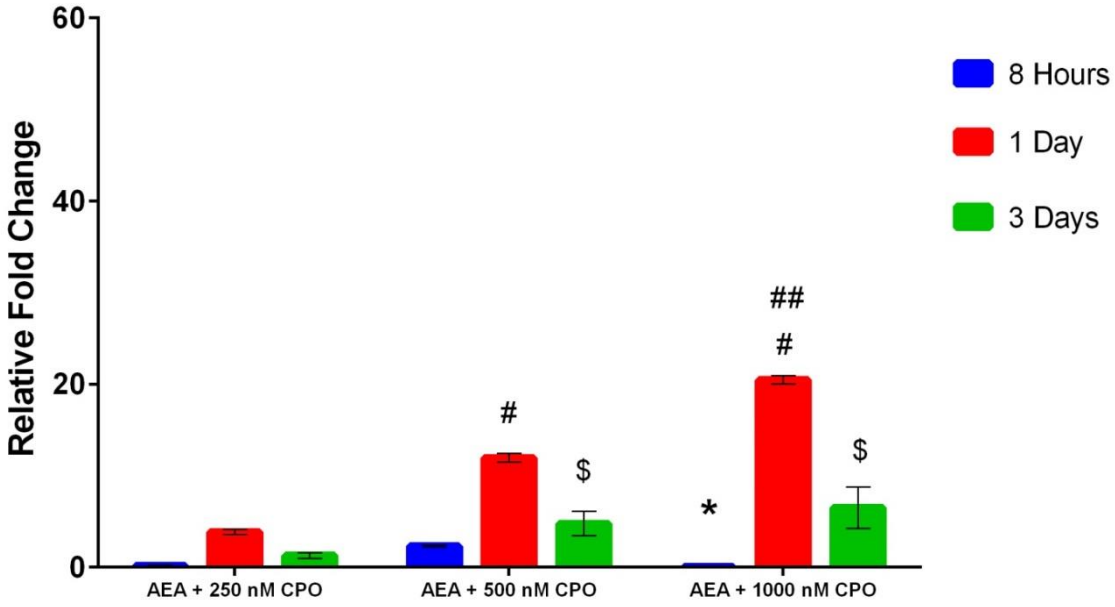

Figure 13. Effects of CPO in the presence of AEA on ACOX1 expression. Relative fold change in expression of ACOX1 over vehicle control after exposure to AEA plus concentrations of chlorpyrifos oxon in culture. Data are presented as mean ± SD. At 8 hours after dosing, a single asterisk indicates a significant difference compared to 250 nM. At 1 day after dosing, a pound sign indicates a significant difference compared to 250 nM while a double pound sign indicates a difference compared to 500 nM. Finally at 3 days after dosing, a dollar sign indicates a difference compared to 250 nM whereas a double dollar sign indicates a difference compared to 500 nM CPO.

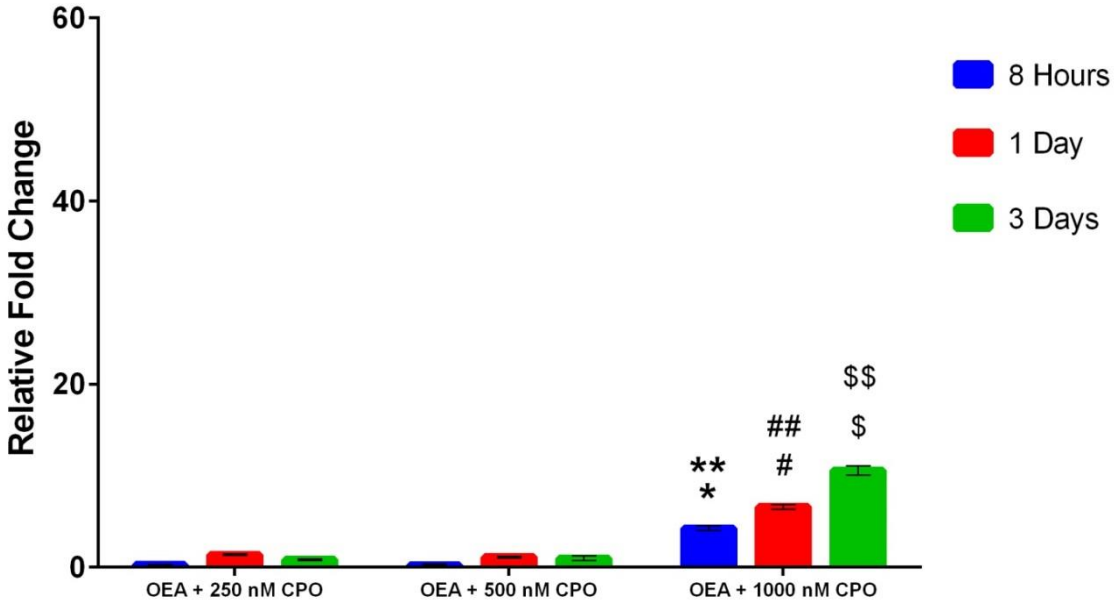

Figure 14. Effects of CPO in the presence of OEA on ACOX1 expression. Relative fold change in expression of ACOX1 over vehicle control after exposure to OEA plus concentrations of chlorpyrifos oxon in culture. Data are presented as mean ± SD. At 8 hours after dosing, a single asterisk indicates a significant difference compared to 250 nM, a double asterisk indicates a significant difference compared to 500 nM. At 1 day after dosing, a pound sign indicates a significant difference compared to 250 nM while a double pound sign indicates a difference compared to 500 nM. Finally at 3 days after dosing, a dollar sign indicates a difference compared to 250 nM, a double dollar sign indicates a difference compared to 500 nM CPO.

	8 Hours	**1Day**	**3 Days**
AEA	0.03 ± 0.01	3.34 ± 0.29	8.28 ± 1.79
OEA	2.98 ± 0.21	1.42 ± 0.09	1.38 ± 0.12

Table 3. Effects of exogenous agonists AEA and OEA on ACOX1 expression in MCF-7 cells. Data are presented as mean relative fold change over vehicle only control, ± SD, n = 3.

AGPAT2

Among the samples from cells treated with CPO alone**,** there was a significant main effect of both CPO ($F_{2,18} = 5.026$, $p = 0.0184$) and time ($F_{2,18} = 12.17$, $p = 0.0005$), however, no significant interaction was noted ($F_{4,18} = 0.533$, $p = 0.7133$). Pairwise comparisons across concentrations revealed a significant difference with 1000 nM CPO after 1 day of exposure.

Additionally, there was a significant main effect of treatment ($F_{3,24} = 245.5$, $p < 0.0001$), and time ($F_{2,24} = 722.9$, $p < 0.0001$), as well as a significant interaction ($F_{6,24} = 142.7$, $p < 0.0001$) for cells treated with AEA only or a combination of AEA and one of the three concentrations of CPO. Pairwise comparisons indicated significant differences among all treatments at 1 day after dosing. The comparisons also determined significant differences between AEA plus 1000 nM CPO and all other treatments among all three durations of exposure.

Finally, in the cells that were treated with OEA alone or a combination of OEA and of three CPO concentrations, there was a significant main effect of treatment ($F_{3,24} = 67$, $p < 0.0001$), and time ($F_{2,24} = 118$, $p < 0.0001$), as well as a significant interaction ($F_{6,24} = 29$, $p < 0.0001$). Pairwise comparisons determined significant differences between OEA alone and all other treatments within the 8 hours exposure period, as well as 1000 nM CPO combined with OEA at 8 hours and 1 day post-dosing time points.

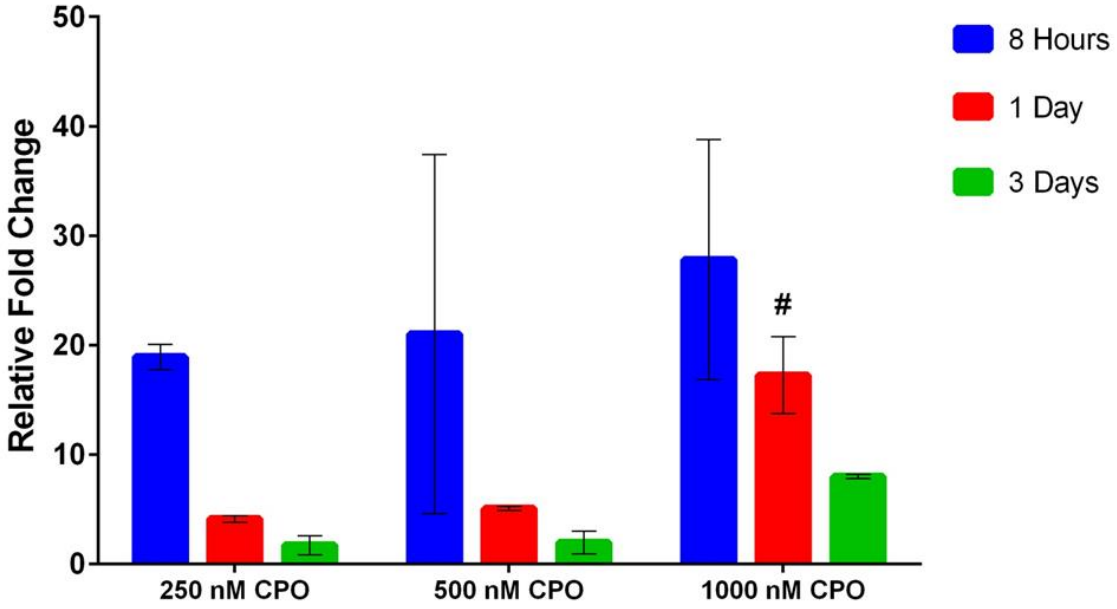

Figure 15. Effects of CPO on AGPAT2 expression. Relative fold change in expression of AGPAT2 over vehicle control with exposure to CPO alone. Data are presented as mean ± SD. At 1 day after dosing, a pound sign indicates a significant difference compared to 250 nM.

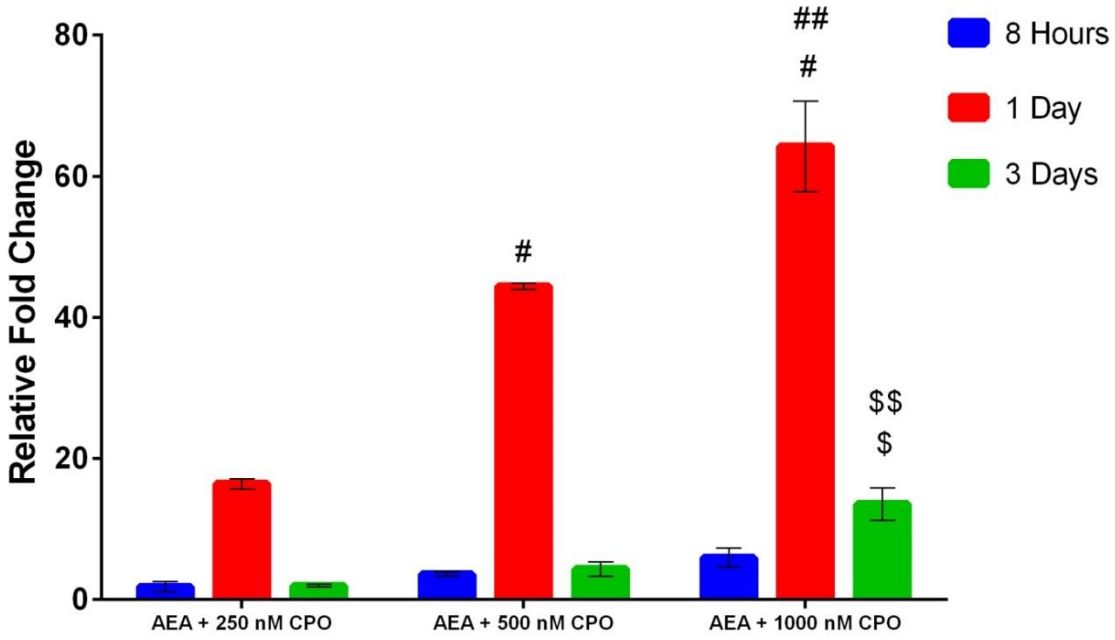

Figure 16. Effects of CPO in the presence of AEA on AGPAT2 expression. Data are presented as mean relative fold change in gene expression ± SD. At 1 day after dosing, a pound sign indicates a significant difference compared to 250 nM while a double pound sign indicates a difference compared to 500 nM. Finally at 3 days after dosing, a dollar sign indicates a difference compared to 250 nM, a double dollar sign indicates a difference compared to 500 nM CPO.

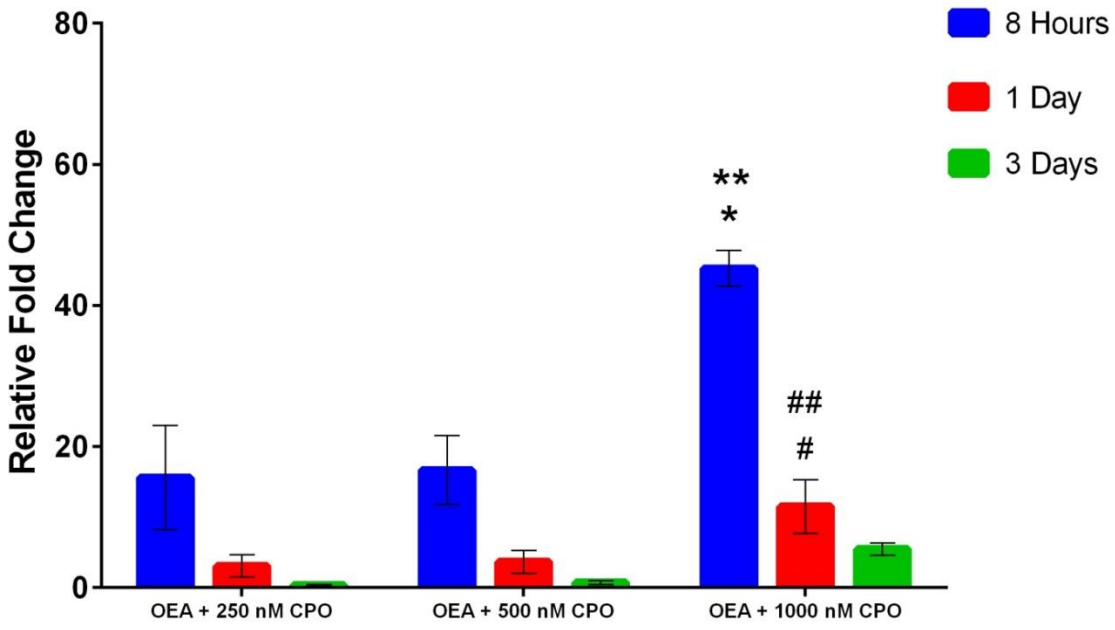

Figure 17. Effects of CPO in the presence of OEA on AGPAT2 expression. Relative fold change in expression of AGPAT2 over vehicle control after exposure to OEA plus concentrations of chlorpyrifos oxon in culture. Data are presented as mean ± SD. At 8 hours after dosing, a single asterisk indicates a significant difference compared to 250 nM, and a double asterisk indicates a significant difference compared to 500 nM. At 1 day after dosing, a pound sign indicates a significant difference compared to 250 nM while a double pound sign indicates a difference compared to 500 nM.

	8 Hours	**1Day**	**3 Days**
AEA	0.27 ± 0.02	4.53 ± 0.68	8.411 ± 0.70
OEA	0.58 ± 0.05	5.01 ± 0.36	0.27 ± 0.01

Table 4. Effects of exogenous agonists AEA and OEA on AGPAT2 expression in MCF-7 cells. Data are presented as mean relative fold change over vehicle only control, $\pm$ SD, n = 3.

ABCG2

There was a significant main effect of both CPO ($F_{2,18} = 494.2$, $p < 0.0001$), and time ($F_{2,18} = 254.2$, $p < 0.0001$), as well as a significant interaction ($F_{4,18} = 147.8$, $p < 0.0001$) found in the samples from cells that were treated only with chlorpyrifos oxon. Pairwise comparisons across concentrations indicated significant differences within each time point, with the exception of no difference of significance between 250 nM and 500 nM CPO 8 hours after dosing.

Among those samples from cells treated with either AEA only, or a combination of AEA and CPO, there was a significant main effect of the treatments ($F_{3,24} = 30.29$, $p < 0.0001$), and time ($F_{2,24} = 26.66$, $p < 0.0001$), as well as a significant interaction ($F_{6,24} = 12.03$, $p < 0.0001$). Pairwise comparisons across all treatments did not determine any significant differences within the 8 hours after dosing time point, but did indicate significant differences between AEA combined with 1000 nM CPO and all other treatments at 1 day after dosing, and that AEA alone and AEA in addition to 1000 nM CPO were both significantly different compared to 250 nM CPO plus AEA at 3 days after dosing.

Lastly, for the cells treated with only OEA or OEA plus one of the three CPO concentrations, there was a significant main effect treatment ($F_{3,24} = 2378$, $p < 0.0001$), and time ($F_{2,24} = 299$, $p < 0.0001$), as well as a significant interaction ($F_{6,24} = 372$, $p < 0.0001$). Pairwise comparisons across all treatments determined significant differences between OEA alone and all other treatments within the 8 hours after dosing period, as

well as 1000 nM CPO combined with OEA to be significantly different compared to all treatments within all three time points.

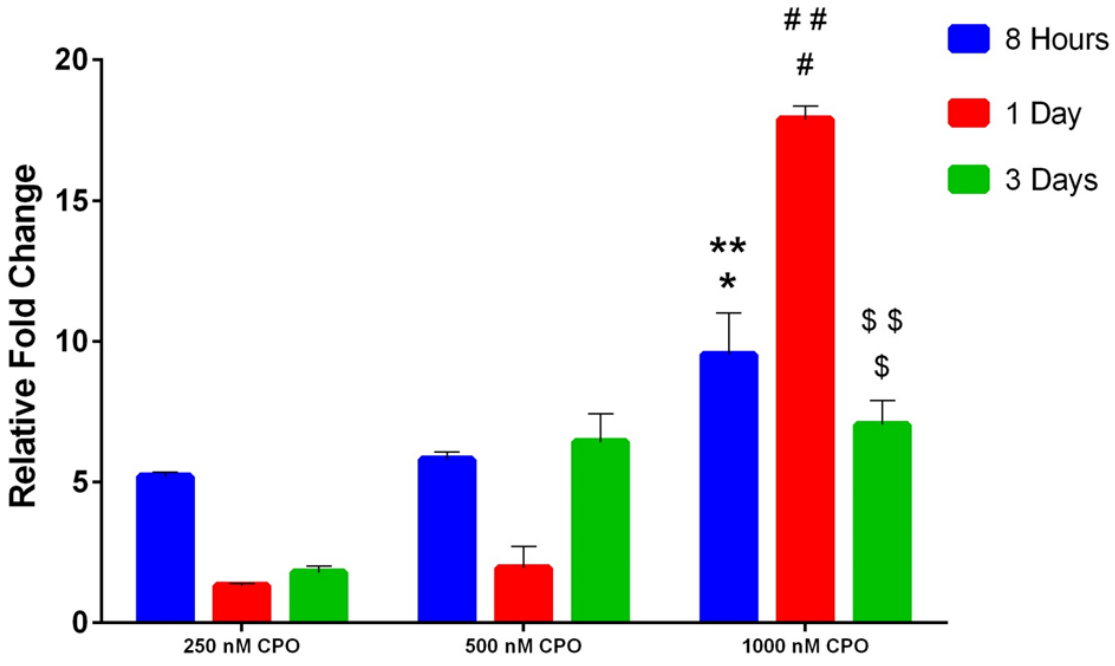

Figure 18. Effects of CPO on ABCG2 expression. Relative fold change in expression of ABCG2 over vehicle control after exposure to CPO alone. Data are presented as mean ± SD. At 8 hours after dosing, a single asterisk indicates a significant difference compared to 250 nM whereas a double asterisk indicates a difference from 500 nM CPO. At 1 day after dosing, a pound sign indicates a significant difference compared to 250 nM while a double pound sign indicates a difference compared to 500 nM. Finally at 3 days after dosing, a dollar sign indicates a difference compared to 250 nM whereas a double dollar sign indicates a difference compared to 500 nM CPO.

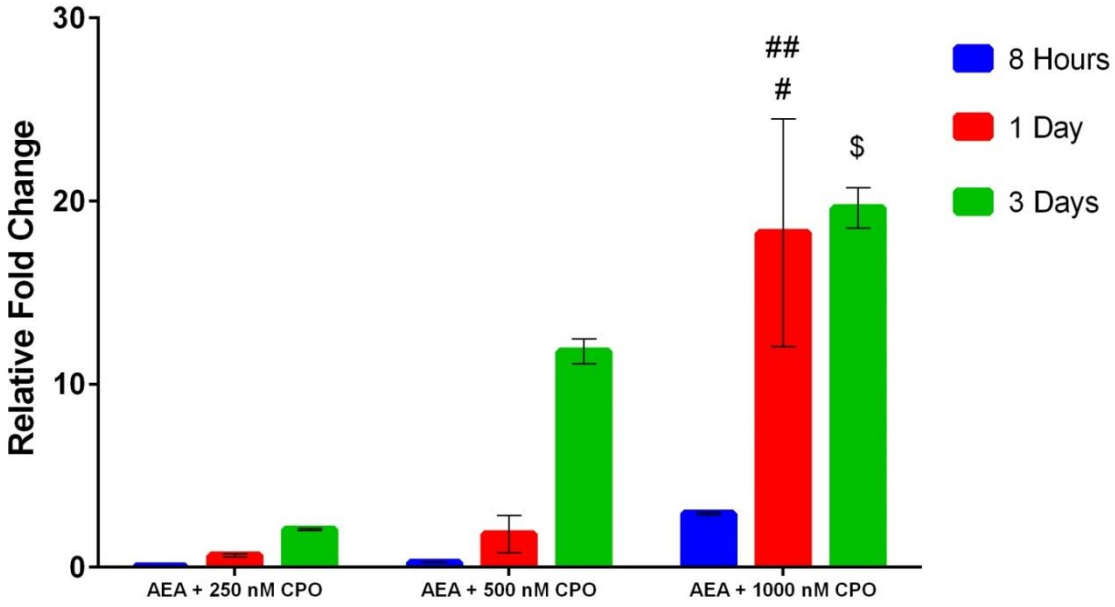

Figure 19. Effects of CPO in the presence of AEA on ABCG2 expression. Relative fold change in expression of ABCG2 over vehicle control after exposure to AEA plus concentrations of chlorpyrifos oxon in culture. Data are presented as mean ± SD. At 1 day after dosing, a pound sign indicates a significant difference compared to 250 nM while a double pound sign indicates a difference compared to 500 nM. At 3 days after dosing, a dollar sign indicates a difference compared to 250 nM.

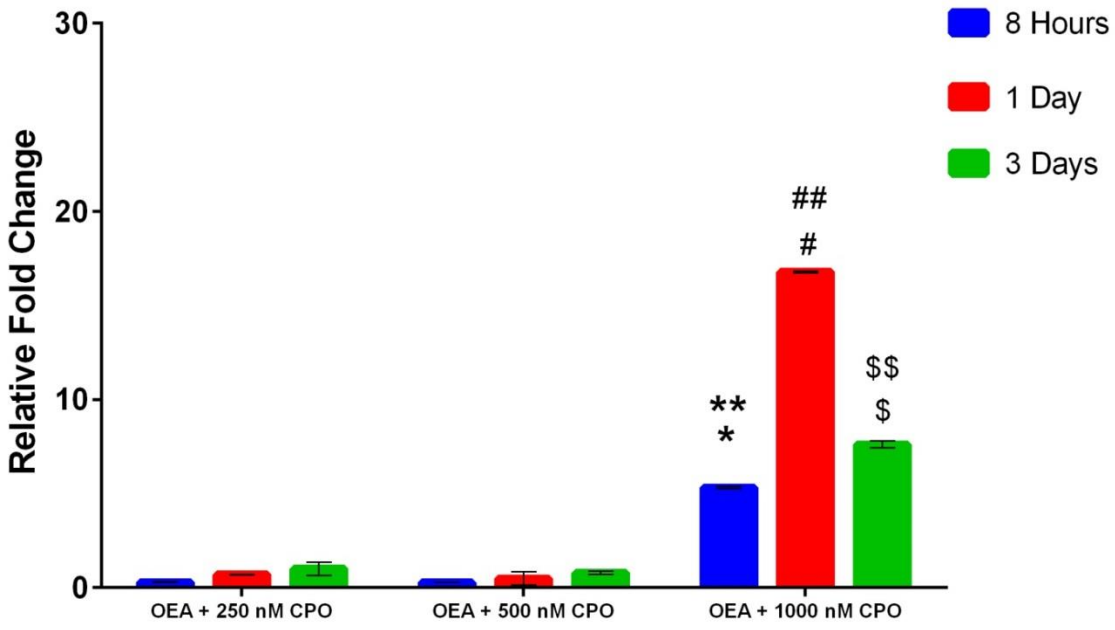

Figure 20 . Effects of CPO in the presence of OEA on ABCG2 expression. Relative fold change in expression of ABCG2 over vehicle control after exposure to OEA plus concentrations of chlorpyrifos oxon in culture. Data are presented as mean ± SD. At 8 hours after dosing, a single asterisk indicates a significant difference compared to 250 nM, and a double asterisk indicates a significant difference compared to 500 nM. At 1 day after dosing, a pound sign indicates a significant difference compared to 250 nM while a double pound sign indicates a difference compared to 500 nM. Finally at 3 days after dosing, a dollar sign indicates a difference compared to 250 nM, a double dollar sign indicates a difference compared to 500 nM CPO.

	8 Hours	**1Day**	**3 Days**
AEA	0.25 ± 0.01	6.28 ± 0.32	9.31 ± 4.48
OEA	1.55 ± 0.07	0.44 ± 0.01	1.37 ± 0.80

Table 5. Effects of AEA and OEA on ABCG2 expression in MCF-7 cells. Data are presented as mean relative fold change over vehicle only control, $\pm$ SD, n = 3.

CHAPTER IV

DISCUSSION

The widespread use of organophosphorus (OP) pesticides is not going away anytime soon. They are efficacious, effective, budget-friendly, and easy to use in their many applications, providing a wide range of benefits to quality of life. Extensive risk assessments and periodic reevaluation have demonstrated that such chemicals can generally be used safely (36). Many of the more hazardous OP pesticides have been removed from use over the last 25 years or so (6). Certain usage restrictions have been imposed based on new data but, overall, chlorpyrifos and other OP pesticides have proven to be both effective and safe. However, it is necessary to examine how these chemicals may impact our health in ways that are not life-threatening or of immediate concern, as part of making sure that benefits continue to outweigh the risks. Despite many investigations into toxicological effects potentially independent of acetylcholinesterase inhibition, there is still much to be learned.

One non-acetylcholinesterase target for OP anticholinesterases that may be particularly important is fatty acid amide hydrolase (FAAH). FAAH is the primary enzyme responsible for inactivation of the endocannabinoid anandamide, as well as

endocannabinoid-like metabolites. A number of studies have reported that FAAH is very sensitive to inhibition by CPO and other OP toxicants.

We hypothesized that inhibition of FAAH by CPO would allow endogenous lipid metabolites (AEA, OEA and/or PEA) to increase activation of PPARs, leading to increased transcriptional activity. We also proposed that the effects of exogenous PPAR agonists would be increased by CPO. Figure 21 illustrates the proposed mechanism by which this could occur. .

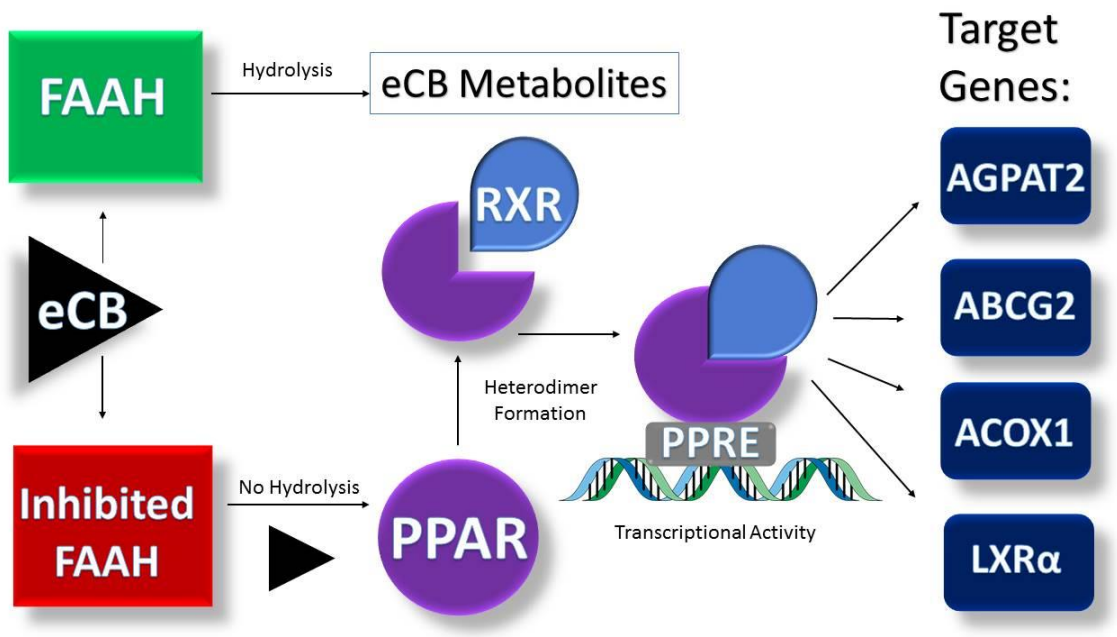

Figure 21. Proposed pathway linking OP exposure to altered expression of PPAR target genes.

Overall, our results showed an upregulation of all selected target genes by CPO. In general, concentration-dependent effects of CPO were noted, with the highest concentration generally causing the greatest increase. Although we predicted that expression changes would occur primarily due to AEA and OEA binding to PPAR, the

results showed that exposure to chlorpyrifos alone also caused significant increases in expression of the target genes. Interestingly, exposure time appeared to differentially affect expression changes among the four genes. AGPAT2 followed most closely our expectations i.e., more extensive changes with greater FAAH inhibition. As FAAH inhibition was greater at the 8 hours and 1 day time point, with substantial recovery at 3 days, we initially expected greater transcriptional changes at the earlier time points. However, both ACOX1 and ABCG2 exhibited the opposite, with gene expression changes. The four genes were initially selected as specific targets for either PPARα (LXRα and ACOX1) or PPARγ (AGPAT2 and ABCG2). However, all four responded to both AEA and OEA exposure, so a clear distinction was not observed in isoform specificity in regulation of the genes in this study. What may be most important however, were the CPO concentration-dependent effects. These data suggest that there is, in fact, a dose-dependent effect on expression changes of at least some PPAR target genes. Such conclusions would be strengthened by performing more experiments with additional genes, followed by investigations that would assist in determining if there are any actual consequences of altered gene expression that could alter physiological function.

Future studies need to be conducted in order to evaluate the physiologic impact of the altered gene expressions that were demonstrated by this study to examine effects on such functions as lipid metabolism. Additional *in vitro* experiments to investigate whether, or not, the observed increased gene expression corresponds to an increase in protein translation are an important step in determining the possible consequences of OP exposure-related PPAR signaling changes. For example, analyses of cell lipid content changes could strengthen conclusions regarding the functional changes associated with

altered gene expression. Such studies could lead to an adverse outcome pathway to describe mechanisms for potential real-life consequences of chronic, low-dose environmental exposure to chlorpyrifos.

The U.S. Centers for Disease Control and Prevention (CDC) National Center for Health Statistics (NCHS) ranks heart disease as the number one cause of death in the United States, with a mortality rate of over 600,000 deaths in 2017 (62). Data from the NCHS 2018 summary reported that roughly 44% of all adults, ages 18 and older, suffer from some form of circulatory compromise, including coronary heart disease and hypertension. High concentrations of plasma cholesterol are a well-known risk factor in the development of cardiovascular disease. As a key regulator of plasma cholesterol levels, as well as intracellular cholesterol, and intestinal cholesterol absorption, dysfunctional expression of LXRα could potentially be a contributor to the ever-increasing incidence of cardiac complications (52,53). Additionally, overexpression of LXRα has been demonstrated to inhibit PPAR binding to RXR, therefore it could also play a role in metabolic disorders by interfering with the roles of PPARs in their regulation of such functions (52,53,63).

The CDC's National Center for Chronic Disease Prevention and Health Promotion estimated in their 2017 report that nearly 10% of the total population of the United States has struggle with diabetes, based on the numbers of known diagnosed to be 23.1 million, and an additional 7.2 million undiagnosed (64). Type 2 diabetes accounts for over 90% of all cases (65). These numbers do not even include the estimated 33.9% of adults aged 18 and older that have been reported to be diagnosed with prediabetes (2015 data). Overexpression of AGPAT2 has been shown to increase triaglycerol

accumulation in the liver, and is a known contributor to development of hepatic steatosis and severe insulin resistance (56,57).

The physiological roles of ABCG2 vary based on tissue-specific location and levels of expression. In all cases, however, ABCG2 is a critical component in regulation of xenobiotic transport both into, and out of, the cells, thereby playing a dual part in protection from toxicants by not allowing absorption, and in homeostasis of cellular functions based on retention or efflux of compounds it transports (58,59). Disruption in normal expression levels of ABCG2 can lead to a number of complications related to xenobiotic absorption and clearance, including altered efficacy of drugs, by increased toxicity due to retention, or even no effect at all, due to resistance to absorption (58).

Continued investigation into the effects of chronic exposure to OP pesticides on non-target organisms and human health is a necessary part of ensuring that the most responsible decisions can be made when it comes to regulation and use of chemicals that we depend on for the protection of vital resources such as food crops, and for the control and prevention of life-threatening diseases spread by target insects like mosquitos and ticks. Although OPs have been extensively studied since they were first synthesized, and careful consideration to detail is made throughout risk assessments in terms of registration and regulation for use in all of their applications, ongoing re-evaluations are important in building the most comprehensive knowledge about such chemicals and their effects on the broader population, in different doses, and over longer periods of time than those typically applied to initial risk assessments and regulatory decisions as their result. While the target genes used in this study, and their representative roles in metabolic functions and disorders are only a miniscule portion of the human metabolome, the

information gathered from these data help to provide a small piece to the much larger puzzle in characterizing the molecular mechanisms in which human health can be affected by elements encountered in our everyday environments.

CHAPTER V

SUMMARY AND CONCLUSIONS

- Both FAAH and AChE in MCF-7 cells were inhibited by CPO in a concentration-dependent manner *in vitro* and *in culture*.
- The expression of four selected genes associated with PPAR signaling showed concentration-dependent increases with CPO exposure.
- Changes in gene expression by CPO could be mediated by FAAH inhibition, leading to PPAR activation by endogenous agonists. In contrast, CPO could act as a direct PPAR agonist. Both of these pathways need further investigation.
- The expression of all four target genes was upregulated with the highest concentration of CPO (1000 nM) when either of the exogenous agonists (AEA or OEA) was included.
- No target gene specificity between PPARα and PPARγ was noted with the exogenous agonists used.
- Gene expression changes appeared to support the hypothesis that FAAH inhibition allows for increased AEA and OEA binding to PPAR, leading to increased PPAR transcriptional activity and upregulation of PPAR target genes.
-

- Additional experiments to investigate corresponding increases in protein products and functional endpoints such as accumulation would strengthen our results.
- Overall, the data suggest a potential link between OP pesticide exposure and altered lipid metabolism, working through PPAR signaling.

REFERENCES

1. Christensen K, Harper B, Luukinen B, Buhl K, Stone D. Chlorpyrifos Technical Fact Sheet [Internet]. National Pesticide Information Center, Oregon State University Extension Services. 2009. Available from: http://npic.orst.edu/factsheets/archive/chlorptech.html#references

2. Costa LG. Organophosphorus Compounds at 80: Some Old and New Issues. Toxicol Sci. 2018 Mar 1;162(1):24–35.

3. Casida JE. Organophosphorus Xenobiotic Toxicology. Annu Rev Pharmacol Toxicol. 2017 Jan 6;57(1):309–27.

4. Casida JE, Quistad GB. Serine hydrolase targets of organophosphorus toxicants. Chem Biol Interact [Internet]. 2005 Dec 15;157–158:277–83. Available from: https://www.sciencedirect.com/science/article/pii/S0009279705002772?via%3Dihub

5. Kondakala S, Lee JH, Ross MK, Howell GE. Effects of acute exposure to chlorpyrifos on cholinergic and non-cholinergic targets in normal and high-fat fed male C57BL/6J mice. Toxicol Appl Pharmacol [Internet]. 2017 Dec 15;337:67–75. Available from: https://www.sciencedirect.com/science/article/pii/S0041008X17304295?via%3Dihub

6. Zeng Z, Yan Y, Wang B, Liu N, Xu H. Discovery and identification of O, O-diethyl O-(4-(5-phenyl-4, 5-dihydroisoxazol-3-yl) phenyl) phosphorothioate (XP-1408) as a novel mode of action of organophosphorus insecticides. Sci Rep. 2017 Dec 1;7(1).

7. Parran DK, Magnin G, Li W, Jortner BS, Ehrich M. Chlorpyrifos alters functional integrity and structure of an in vitro BBB model: Co-cultures of bovine endothelial cells and neonatal rat astrocytes. Neurotoxicology. 2005;26(1):77–88.

8. Huang H-M, Pai M-H, Liu J-J, Yeh S-L, Hou Y-C. Effects of dietary exposure to chlorpyrifos on immune cell populations and inflammatory responses in mice with dextran sulfate sodium-induced colitis. Food Chem Toxicol [Internet]. 2019 Sep 1;131:110596. Available from: https://www.sciencedirect.com/science/article/pii/S0278691519303850?via%3Dihub

9. Crane AL, Klein K, Olson JR. Bioactivation of chlorpyrifos by CYP2B6 variants. Xenobiotica. 2012 Dec;42(12):1255–62.

10. Sultatos LG. Concentration-dependent binding of chlorpyrifos oxon to acetylcholinesterase. Toxicol Sci. 2007 Nov;100(1):128–35.

11. Scheffel C, Niessen K V., Rappenglück S, Wanner KT, Worek F, Seeger T. Counteracting desensitization of human α7-nicotinic acetylcholine receptors with bispyridinium compounds as an approach against organophosphorus poisoning. Toxicol Lett [Internet]. 2018 Sep 1;293:149–56. Available from: https://www.sciencedirect.com/science/article/pii/S0378427417315151?via%3Dihub

12. Carr RL, Graves CA, Mangum LC, Nail CA, Ross MK. Low level chlorpyrifos exposure increases anandamide accumulation in juvenile rat brain in the absence of brain cholinesterase inhibition. Neurotoxicology [Internet]. 2014 Jul 1;43:82–9. Available from: https://www.sciencedirect.com/science/article/pii/S0161813X13001903?via%3Dihub

13. Casida JE, Quistad GB. Organophosphate toxicology: Safety aspects of nonacetylcholinesterase secondary targets. Vol. 17, Chemical Research in Toxicology.

2004. p. 983–98.

14. Nomura DK, Casida JE. Activity-based protein profiling of organophosphorus and thiocarbamate pesticides reveals multiple serine hydrolase targets in mouse brain. J Agric Food Chem. 2011 Apr 13;59(7):2808–15.

15. Huang H, Nishi K, Tsai H-J, Hammock BD. Development of highly sensitive fluorescent assays for fatty acid amide hydrolase. Anal Biochem [Internet]. 2007 Apr 1 [cited 2019 Oct 7];363(1):12–21. Available from: https://www.sciencedirect.com/science/article/pii/S0003269706008049?via%3Dihub

16. Ueda N, Puffenbarger RA, Yamamoto S, Deutsch DG. The fatty acid amide hydrolase (FAAH). Chem Phys Lipids [Internet]. 2000 Nov 1;108(1–2):107–21. Available from: https://www.sciencedirect.com/science/article/pii/S0009308400001900?via%3Dihub

17. Nallapaneni A, Liu J, Karanth S, Pope C. Pharmacological enhancement of endocannabinoid signaling reduces the cholinergic toxicity of diisopropylfluorophosphate. Neurotoxicology [Internet]. 2008 Nov 1;29(6):1037–43. Available from: https://www.sciencedirect.com/science/article/pii/S0161813X08001423?via%3Dihub

18. Liu J, Pope C. The cannabinoid receptor antagonist AM251 increases paraoxon and chlorpyrifos oxon toxicity in rats. Neurotoxicology [Internet]. 2015 Jan 1;46:12–8. Available from: https://www.sciencedirect.com/science/article/pii/S0161813X14001843?via%3Dihub

19. Quistad GB, Klintenberg R, Caboni P, Liang SN, Casida JE. Monoacylglycerol lipase inhibition by organophosphorus compounds leads to elevation of brain 2-arachidonoylglycerol and the associated hypomotility in mice. Toxicol Appl Pharmacol [Internet]. 2006 Feb 15;211(1):78–83. Available from:

https://www.sciencedirect.com/science/article/pii/S0041008X05006162?via%3Dihub

20. Mangas I, Estevez J, Vilanova E, França TCC. New insights on molecular interactions of organophosphorus pesticides with esterases. Toxicology [Internet]. 2017 Feb 1;376:30–43. Available from: https://www.sciencedirect.com/science/article/pii/S0300483X16300956?via%3Dihub

21. McKinney MK, Cravatt BF. Structure and Function of Fatty Acid Amide Hydrolase. Annu Rev Biochem. 2005 Jun;74(1):411–32.

22. Grotenhermen F. Pharmacokinetics and pharmacodynamics of cannabinoids. Clin Pharmacokinet [Internet]. 2003 [cited 2019 Sep 30];42(4):327–60. Available from: http://link.springer.com/10.2165/00003088-200342040-00003

23. Mechoulam R, Hanuš LO, Pertwee R, Howlett AC. Early phytocannabinoid chemistry to endocannabinoids and beyond. Vol. 15, Nature Reviews Neuroscience. Nature Publishing Group; 2014. p. 757–64.

24. Devane WA, Hanuš L, Breuer A, Pertwee RG, Stevenson LA, Griffin G, et al. Isolation and structure of a brain constituent that binds to the cannabinoid receptor. Science (80-). 1992;258(5090):1946–9.

25. Osei-Hyiaman D, DePetrillo M, Pacher P, Liu J, Radaeva S, Bátkai S, et al. Endocannabinoid activation at hepatic CB1 receptors stimulates fatty acid synthesis and contributes to diet-induced obesity. J Clin Invest [Internet]. 2005 May 2 [cited 2019 Oct 7];115(5):1298–305. Available from: http://www.jci.org/articles/view/23057

26. Baireddy P, Liu J, Hinsdale M, Pope C. Comparative effects of chlorpyrifos in wild type and cannabinoid Cb1 receptor knockout mice. Toxicol Appl Pharmacol [Internet]. 2011 Nov 1;256(3):324–9. Available from:

https://www.sciencedirect.com/science/article/pii/S0041008X11002092?via%3Dihub

27. Castillo PE, Younts TJ, Chávez AE, Hashimotodani Y. Endocannabinoid Signaling and Synaptic Function. Neuron [Internet]. 2012 Oct 4;76(1):70–81. Available from: https://www.sciencedirect.com/science/article/pii/S0896627312008550?via%3Dihub

28. Tegeder I. Endocannabinoids as guardians of metastasis. Vol. 17, International Journal of Molecular Sciences. MDPI AG; 2016.

29. Di Marzo V, Fontana A, Cadas H, Schinelli S, Cimino G, Schwartz JC, et al. Formation and inactivation of endogenous cannabinoid anandamide in central neurons. Nature. 1994;372(6507):686–91.

30. Brunetti L, Loiodice F, Piemontese L, Tortorella P, Laghezza A. New Approaches to Cancer Therapy: Combining Fatty Acid Amide Hydrolase (FAAH) Inhibition with Peroxisome Proliferator-Activated Receptors (PPARs) Activation. J Med Chem. 2019 Aug 22;

31. Mandard S, Müller M, Kersten S. Peroxisome proliferator-activated receptor α target genes. Vol. 61, Cellular and Molecular Life Sciences. 2004. p. 393–416.

32. Semple RK, Chatterjee VKK, O'Rahilly S. PPARγ and human metabolic disease. Vol. 116, Journal of Clinical Investigation. 2006. p. 581–9.

33. Spire C, Rogue A, Brun M, Claude N, Guillouzo A. Gene expression changes induced by PPAR gamma agonists in animal and human liver. PPAR Research. Hindawi Limited; 2010.

34. Grygiel-Górniak B. Peroxisome proliferator-activated receptors and their ligands: Nutritional and clinical implications - A review. Nutr J. 2014 Feb 14;13(1).

35. Shaffo FC, Grodzki AC, Fryer AD, Lein PJ. Mechanisms of organophosphorus pesticide toxicity in the context of airway hyperreactivity and asthma. Vol. 315, American Journal of Physiology - Lung Cellular and Molecular Physiology. American Physiological Society; 2018. p. L485–501.

36. Naughton SX, Terry A V. Neurotoxicity in acute and repeated organophosphate exposure. Toxicology [Internet]. 2018 Sep 1;408:101–12. Available from: https://www.sciencedirect.com/science/article/pii/S0300483X18302646?via%3Dihub

37. Jiang W, Duysen EG, Hansen H, Shlyakhtenko L, Schopfer LM, Lockridge O. Mice treated with chlorpyrifos or chlorpyrifos oxon have organophosphorylated tubulin in the brain and disrupted microtubule structures, suggesting a role for tubulin in neurotoxicity associated with exposure to organophosphorus agents. Toxicol Sci. 2010 May;115(1):183–93.

38. Zheng Q. Comparative Cholinergic Neurotoxicity of Oral Chlorpyrifos Exposures in Preweanling and Adult Rats. Toxicol Sci. 2000 May 1;55(1):124–32.

39. Fang B, Li JW, Zhang M, Ren FZ, Pang GF. Chronic chlorpyrifos exposure elicits diet-specific effects on metabolism and the gut microbiome in rats. Food Chem Toxicol. 2018 Jan 1;111:144–52.

40. Rezg R, Mornagui B, El-Fazaa S, Gharbi N. Organophosphorus pesticides as food chain contaminants and type 2 diabetes: a review. Trends Food Sci Technol [Internet]. 2010 Jul 1;21(7):345–57. Available from: https://www.sciencedirect.com/science/article/pii/S0924224410001081?via%3Dihub

41. Ndonwi EN, Atogho-Tiedeu B, Lontchi-Yimagou E, Shinkafi TS, Nanfa D, Balti E V., et al. Gestational Exposure to Pesticides Induces Oxidative Stress and Lipid Peroxidation in

Offspring that Persist at Adult Age in an Animal Model. Toxicol Res. 2019 Jul 15;35(3):241–8.

42. Lasram MM, Dhouib IB, Annabi A, El Fazaa S, Gharbi N. A review on the molecular mechanisms involved in insulin resistance induced by organophosphorus pesticides. Toxicology [Internet]. 2014 Aug 1 [cited 2019 Oct 7];322:1–13. Available from: https://www.sciencedirect.com/science/article/pii/S0300483X14000936?via%3Dihub

43. Finkelstein EA, Trogdon JG, Cohen JW, Dietz W. Annual medical spending attributable to obesity: Payer-and service-specific estimates. Health Aff. 2009 Sep;28(5).

44. Hales CM, Carroll MD, Fryar CD, Ogden CL. Prevalence of Obesity Among Adults and Youth: United States, 2015-2016 Key findings Data from the National Health and Nutrition Examination Survey [Internet]. 2015. Available from: https://www.cdc.gov/nchs/data/databriefs/db288_table.pdf#1.

45. Desvergne B, Feige JN, Casals-Casas C. PPAR-mediated activity of phthalates: A link to the obesity epidemic? Mol Cell Endocrinol [Internet]. 2009 May 25 [cited 2019 Oct 11];304(1–2):43–8. Available from: https://www.sciencedirect.com/science/article/pii/S030372070900149X

46. Fang M, Webster TF, Ferguson PL, Stapleton HM. Characterizing the Peroxisome Proliferator-Activated Receptor (PPAR γ) Ligand Binding Potential of Several Major Flame Retardants, Their Metabolites, and Chemical Mixtures in House Dust. Environ Health Perspect [Internet]. 2015 Feb [cited 2019 Oct 11];123(2):166–72. Available from: https://ehp.niehs.nih.gov/doi/10.1289/ehp.1408522

47. Atrice Desvergne B, Michalik L, Wahli W. Transcriptional Regulation of Metabolism. 2006 [cited 2019 Oct 14]; Available from: www.prv.org

48. Strand E, Lysne V, Grinna ML, Bohov P, Svardal A, Nygård O, et al. Short-Term Activation of Peroxisome Proliferator-Activated Receptors α and γ Induces Tissue-Specific Effects on Lipid Metabolism and Fatty Acid Composition in Male Wistar Rats. PPAR Res. 2019;2019.

49. Xu P, Zhai Y, Wang J. The role of PPAR and its cross-talk with CAR and LXR in obesity and atherosclerosis. Vol. 19, International Journal of Molecular Sciences. MDPI AG; 2018.

50. Savage DB. PPARγ as a metabolic regulator: Insights from genomics and pharmacology. Vol. 7, Expert Reviews in Molecular Medicine. 2005.

51. Human Protein Atlas [Internet]. Available from: http://www.proteinatlas.org

52. Robitaille J, Houde A, Lemieux S, Gaudet D, Pérusse L, Vohl MC. The lipoprotein/lipid profile is modulated by a gene-diet interaction effect between polymorphisms in the liver X receptor-α and dietary cholesterol intake in French-Canadians. Br J Nutr. 2007 Jan;97(1):11–8.

53. Yoshikawa T, Ide T, Shimano H, Yahagi N, Amemiya-Kudo M, Matsuzaka T, et al. Cross-talk between peroxisome proliferator-activated receptor (PPAR) α and liver X receptor (LXR) in nutritional regulation of fatty acid metabolism. I. PPARS suppress sterol regulatory element binding protein-1c promoter through inhibition of LXR signali. Mol Endocrinol. 2003 Jul 1;17(7):1240–54.

54. Varanasi U, Chu R, Chu S, Espinosa R, Lebeau MM, Reddy JK. Isolation of the human peroxisomal acyl-CoA oxidase gene: Organization, promoter analysis, and chromosomal localization. Proc Natl Acad Sci U S A. 1994 Apr 12;91(8):3107–11.

55. Oaxaca-Castillo D, Andreoletti P, Vluggens A, Yu S, van Veldhoven PP, Reddy JK, et al.

Biochemical characterization of two functional human liver acyl-CoA oxidase isoforms 1a and 1b encoded by a single gene. Biochem Biophys Res Commun [Internet]. 2007 Aug 24;360(2):314–9. Available from: https://www.sciencedirect.com/science/article/pii/S0006291X07012156?via%3Dihub

56. Agarwal AK, Sukumaran S, Cortés VA, Tunison K, Mizrachi D, Sankella S, et al. Human 1-Acylglycerol-3-phosphate O-Acyltransferase isoforms 1 and 2: Biochemical characterization and inability to rescue hepatic steatosis in Agpat2 -/- gene lipodystrophic mice. J Biol Chem. 2011 Oct 28;286(43):37676–91.

57. Haque W, Garg A, Agarwal AK. Enzymatic activity of naturally occurring 1-acylglycerol-3-phosphate-O-acyltransferase 2 mutants associated with congenital generalized lipodystrophy. Biochem Biophys Res Commun [Internet]. 2005 Feb 11;327(2):446–53. Available from: https://www.sciencedirect.com/science/article/pii/S0006291X04027925?via%3Dihub

58. Peña-Solórzano D, Stark SA, König B, Sierra CA, Ochoa-Puentes C. ABCG2/BCRP: Specific and Nonspecific Modulators. Vol. 37, Medicinal Research Reviews. John Wiley and Sons Inc.; 2017. p. 987–1050.

59. Kusuhara H, Sugiyama Y. ATP-binding cassette, subfamily G (ABCG family). Vol. 453, Pflugers Archiv European Journal of Physiology. 2007. p. 735–44.

60. Bradford MM. A rapid and sensitive method for the quantitation of microgram quantities of protein utilizing the principle of protein-dye binding. Anal Biochem. 1976 May 7;72(1–2):248–54.

61. Ellman GL, Courtney KD, Andres V, Featherstone RM. A new and rapid colorimetric determination of acetylcholinesterase activity. Biochem Pharmacol [Internet]. 1961 Jul

1;7(2):88–95. Available from: https://www.sciencedirect.com/science/article/abs/pii/0006295261901459?via%3Dihub

62. Fast Stats - Heart Disease [Internet]. Centers for Disease Control - National Center for Health Satistics. Available from: https://www.cdc.gov/nchs/fastats/heart-disease.htm

63. Willy PJ, Umesono K, Ong ES, Evans RM, Heyman RA, Mangelsdorf DJ. LXR, a nuclear receptor that defines a distinct retinoid response pathway. Genes Dev. 1995 May 1;9(9):1033–45.

64. Centers for Disease Control. National Diabetes Statistics Report, 2017 Estimates of Diabetes and Its Burden in the United States Background. 2017.

65. Porskjær Christensen L, Bahij El-Houri R. Development of an In Vitro Screening Platform for the Identification of Partial PPARγ Agonists as a Source for Antidiabetic Lead Compounds. Vol. 23, Molecules (Basel, Switzerland). NLM (Medline); 2018.

VITA

Stacey Herriage

Candidate for the Degree of

Master of Science

Thesis: IN VITRO EFFECTS OF CHLORPYRIFOS OXON ON PEROXISOME PROLIFERATOR-ACTIVATED SIGNALING IN MCF-7 CELLS

Major Field: Veterinary Biomedical Sciences

Biographical:

Education:

Completed the requirements for the Master of Science in Veterinary Biomedical Sciences at Oklahoma State University, Stillwater, Oklahoma in December, 2019.

Completed the requirements for the Bachelor of Arts in General Studies at Northeastern State University, Tahlequah, Oklahoma in 2013.

Experience:

Graduate Research Assistant in the department of Physiological Sciences, Neurotoxicology Lab, Oklahoma State University, Stillwater, Oklahoma since June 2017.

Professional Memberships:

Society of Toxicology